Neurobiology of Disease 158 (2021) 105468

Contents lists available at ScienceDirect

Neurobiology of Disease

journal homepage: www.elsevier.com/locate/ynbdi

CXCL1-CXCR1/2 signaling is induced in human temporal lobe epilepsy and contributes to seizures in a murine model of acquired epilepsy

Rossella Di Sapia [a], Till S. Zimmer [b], Valentina Kebede [a], Silvia Balosso [a], Teresa Ravizza [a], Diletta Sorrentino [a], Manuel Alejandro Montano Castillo [a], Luca Porcu [c], Franca Cattani [d], Anna Ruocco [d], Eleonora Aronica [b,e], Marcello Allegretti [d], Laura Brandolini [d,1], Annamaria Vezzani [a,*,1]

[a] Department of Neuroscience, Istituto di Ricerche Farmacologiche Mario Negri IRCCS, Italy
[b] Department of Neuropathology, Amsterdam UMC, Amsterdam Neuroscience, Amsterdam, the Netherlands
[c] Department of Oncology, Istituto di Ricerche Farmacologiche Mario Negri IRCCS, Italy
[d] R&D Department, Dompé farmaceutici S.p.A., L'Aquila, Italy
[e] Stichting Epilepsie Instellingen Nederland (SEIN), Heemstede, the Netherlands

ARTICLE INFO

Keywords:
Chemokine
Glia
Neuroinflammation
Neurodegeneration
Reparixin
Status epilepticus

ABSTRACT

CXCL1, a functional murine orthologue of the human chemokine CXCL8 (IL-8), and its CXCR1 and CXCR2 receptors were investigated in a murine model of acquired epilepsy developing following status epilepticus (SE) induced by intra-amygdala kainate. CXCL8 and its receptors were also studied in human temporal lobe epilepsy (TLE). The functional involvement of the chemokine in seizure generation and neuronal cell loss was assessed in mice using reparixin (formerly referred to as repertaxin), a non-competitive allosteric inhibitor of CXCR1/2 receptors.

We found a significant increase in hippocampal CXCL1 level within 24 h of SE onset that lasted for at least 1 week. No changes were measured in blood. In analogy with human TLE, immunohistochemistry in epileptic mice showed that CXCL1 and its two receptors were increased in hippocampal neuronal cells. Additional expression of these molecules was found in glia in human TLE.

Mice were treated with reparixin or vehicle during SE and for additional 6 days thereafter, using subcutaneous osmotic minipumps. Drug-treated mice showed a faster SE decay, a reduced incidence of acute symptomatic seizures during 48 h post-SE, and a delayed time to spontaneous seizures onset compared to vehicle controls. Upon reparixin discontinuation, mice developed spontaneous seizures similar to vehicle mice, as shown by EEG monitoring at 14 days and 2.5 months post-SE. In the same epileptic mice, reparixin reduced neuronal cell loss in the hippocampus vs vehicle-injected mice, as assessed by Nissl staining at completion of EEG monitoring.

Reparixin administration for 2 weeks in mice with established chronic seizures, reduced by 2-fold on average seizure number vs pre-treatment baseline, and this effect was reversible upon drug discontinuation. No significant changes in seizure number were measured in vehicle-injected epileptic mice that were EEG monitored in parallel.

Abbreviations: AP, alkaline phosphatase; BBB, blood brain barrier; BCA, bicinchoninic acid; BSA, bovine serum albumin; CA, cornu ammonis; CSF, cerebrospinal fluid; CCL2, chemokine (C—C motif) ligand 2; CCR, C-C chemokine receptor; CXCL1, chemokine (C-X-C motif) ligand 1; CXCR, CXC chemokine receptors; CX3CL1, chemokine (C-X3-C motif); EDTA, ethylenediaminetetraacetic acid; EEG, electroencephalography; EGTA, ethylene glycol tetraacetic acid; ESI, electrospray ionization; GABA, gamma-aminobutyric acid; GC, granule cells; GFAP, glial fibrillary acidic protein; GLT-1, glutamate transporter 1; h, hilus; $Kir_{4.1}$, inward rectifying potassium channel 4.1; HPLC, high performance liquid chromatography; HRP, horseradish peroxidase; HS, hippocampal sclerosis; IL-8, interleukin 8; MIP-2, macrophage inflammatory protein-2; MMP9, matrix metallopeptidase 9; MS, mass spectrometer; NMDAR, *N*-methyl-D-aspartate receptors; NORSE, new onset refractory status epilepticus; OD, optical density; PBS, phosphate buffered solution; PFA, paraformaldehyde; PMSF, phenylmethylsulfonyl fluoride; SDS-PAGE, sodium dodecyl sulphate - polyacrylamide *gel electrophoresis*; SE, status epilepticus; Sub, subiculum; TLE, temporal lobe epilepsy; TRPV1, transient receptor potential vanilloid 1.

* Corresponding author at: Department of Neuroscience, Istituto di Ricerche Farmacologiche Mario Negri IRCCS, Via Mario Negri 2, Milano, Italy.
E-mail address: annamaria.vezzani@marionegri.it (A. Vezzani).

[1] Shared last authorship

https://doi.org/10.1016/j.nbd.2021.105468
Received 18 June 2021; Received in revised form 20 July 2021; Accepted 2 August 2021
Available online 4 August 2021

Data show that CXCL1-IL-8 signaling is activated in experimental and human epilepsy and contributes to acute and chronic seizures in mice, therefore representing a potential new target to attain anti-ictogenic effects.

1. Introduction

CXCL1, also known as Gro/KC, is a functional murine orthologue of the human chemokine CXCL8 (i.e., IL-8). The chemokine is best known for its role in neutrophil chemotaxis and degranulation during inflammation (Baggiolini, 1998). However, CXCL1 also has direct effects on neuronal function in both peripheral and central nervous systems by activating its cognate G-protein coupled CXCR1 and CXCR2 receptors expressed by neurons. In particular, acute application of the chemokine to dorsal root ganglion neurons induced an intracellular Ca^{2+} elevation, likely due to activation of TRPV1 receptors (Deftu et al., 2018; Qin et al., 2005), and markedly increased Na^{+} currents after a prolonged application (Wang et al., 2008). These effects were associated with enhanced neuronal excitability, and causally linked to CXCL1 involvement in neuropathic pain. CXCL1 was also shown to enhance synaptic transmission in the anterior cingulate cortex by increasing probability of neurotransmitter release (Cui et al., 2012). Notably, there is evidence of a functional interaction between CXCL1 and neuronal *N*-methyl-D-aspartate receptors (NMDAR). Specifically, the CXCL1-CXCR2 axis contributes to inflammatory pain through activation of NMDAR in the spinal cord (Cao et al., 2014), mediated by upregulation of NR2B-containing NMDA receptor expression and phosphorylation (Yang et al., 2016).

These observations establish a potential link between CXCL1 and neuronal hyperexcitability underlying seizures in epilepsy. In fact, a neuroinflammatory *milieu* of chemokines, cytokines, prostaglandins and other inflammatory mediators are induced in brain resident cells in seizure foci from structural/acquired forms of human epilepsy. Importantly, neuroinflammation contributes to experimental seizure onset and recurrence (Vezzani et al., 2019). Pivotal mechanisms of hyperexcitability involve rapid-onset functional interactions between some inflammatory molecules and glutamate or GABA receptors, and modulation by cytokines and chemokines of voltage-gated ion channels and neurotransmitter release (Frigerio et al., 2018a; Vezzani et al., 2019; Vezzani and Viviani, 2015).

The potential link between CXCL8/IL-8 and human epilepsy is reinforced by evidence of increased chemokine expression in microglia and astrocytes in human mesial TLE foci (Morin-Brureau et al., 2018; Pernhorst et al., 2013; Strauss and Elisevich, 2016), and in patients with chronic intractable epilepsy (Choi et al., 2009). Moreover, IL-8 was increased in cerebrospinal fluid (CSF) or serum of patients with status epilepticus or drug resistant seizures (Gallentine et al., 2017; Taalab et al., 2019; Pollard et al., 2013; Sakuma et al., 2014), and in saliva of children with acute seizures (Bartolini et al., 2018). When different epilepsy etiology groups were compared, IL-8 was commonly increased as shown by whole-genome mRNA expression profile in whole blood (Rawat et al., 2020). Finally, IL-8 levels in CSF or serum were reduced in patients responding to therapeutic anti-seizure interventions (De Herdt et al., 2009; Kenney-Jung et al., 2016).

Based on this data, our main goal was to investigate whether the CXCL1-CXCR1/CXCR2 axis was activated in epilepsy and played a role in seizure generation in a murine model of TLE.

The CXCL1 contribution to seizures was assessed by treating mice with reparixin, an allosteric inhibitor of CXCR1/2 receptors. Previous in vitro studies showed that reparixin specifically blocks human neutrophils migration induced by CXCL8 (IC50 = 1 nM) and CXCL1 (IC50 = 400 nM), and rodent neutrophils chemotaxis induced by CXCL1 and CXCL2 without showing any effect on the leukocyte migration induced by other chemoattractants (Bertini et al., 2004). The specificity of the compound was also proven in preventing neutrophil recruitment and tissue damage in animal models of brain ischemia/reperfusion (Bertini et al., 2004; Souza et al., 2004), and lung injury (Zarbock et al., 2008).

In the present study, the compound was administered either before spontaneous seizure onset or in chronic disease. We also investigated IL-8 and its receptors expression in brain specimens from TLE patients.

Data provide novel evidence that reparixin reduces seizures in mice thus implying that CXCL1 has ictogenic actions. We also show that the IL-8 signaling pathway is induced in human epilepsy. Since reparixin is an investigational drug with a safe and well-tolerated profile in humans, the IL-8 axis represents a druggable target with potential translational relevance for attaining anti-seizure effects.

2. Materials and methods

2.1. Animal housing and ethical approval

C57BL/6 N male mice (8 week-old, 25–30 g) were used (Charles River, Calco, Italy). Mice were housed (5 mice in each cage) in the SPF facility at constant room temperature (23 °C) and relative humidity (60 ± 5%) with free access to food (VRF1 diet, Charles River) and water, and with a fixed 12 h light/dark cycle.

After mice were exposed to surgery for EEG set up implantation, they were individually housed with environmental enrichment in their cage (e.g., nesting material including toilet paper and straw; Hutchinson et al., 2005). Animal experiments were designed in accordance with Animal Research Reporting of In Vivo Experiments (ARRIVE) guidelines (Kilkenny et al., 2010**).** All efforts were made to minimize the number of animals used and their suffering according to the principles of the 3Rs (Replacement, Reduction and Refinement; *https://www.nc3rs.org.uk/the-3rs*). Experimental procedures were conducted in conformity with institutional guidelines, in compliance with national (D.L. n.26, G. U. March 4, 2014) and international guidelines and laws (EEC Council Directive 86/609, OJ L 358, 1, December 12, 1987, Guide for the Care and Use of Laboratory Animals, U.S. National Research Council, 1996), and reviewed and approved by the intramural ethical committee.

2.2. Stereotaxic surgery

Mice were surgically implanted under general gas anaesthesia (1–3% isoflurane in O_2) and stereotaxic guidance. A 23-gauge guide cannula was unilaterally positioned on top of the *dura mater* for the intra-amygdala injection of kainic acid (KA) (from bregma, mm: nose bar 0; anteroposterior, −0.9; lateral, −3.1) (Iori et al., 2017). In mice killed 7 days post-SE, cortical electrodes were placed bilaterally onto the somatosensory cortex (from bregma, mm: anteroposterior, −1.8; lateral, ±1.4). In mice undergoing chronic EEG monitoring, a bipolar Teflon-insulated stainless-steel depth electrode (60 μm OD) was implanted in the septal pole of the hippocampus (from bregma, mm: nose bar 0; anteroposterior −1.8, lateral 1.4 and 1.8 below dura mater) contralateral to the injected amygdala, and a cortical electrode was placed onto the somatosensory cortex in the ipsilateral hemisphere. Finally, ground and reference electrodes were positioned over the nasal sinus and the cerebellum, respectively. Electrodes were connected to a multipin socket and secured to the skull by acrylic dental cement. Electrode-implanted mice not exposed to SE were used as sham controls. At the end of stereotaxic surgery, we carried out perioperative analgesia by treating mice with buprenorphine (Bupaq, 0.1 mg/kg, s.c; Alcyon Italia S.p.a., Cherasco, CN, Italy) once-a-day for 3 consecutive days.

2.3. Status epilepticus induction

One week after surgery, mice were connected to the EEG set up (TWIN EEG recording system; version 4.5.3.23) connected with a Comet AS-40 32/8 Amplifier (sampling rate 400 Hz, high-pass filter 0.3 Hz, low-pass filter 70 Hz, sensitivity 2000 mv/cm; Grass-telefactor, West Warwick, RI, USA) for at least 24 h in order to record an EEG baseline before the induction of status epilepticus (SE). Kainic acid (0.3 μg in 0.2 μl; Sigma-Aldrich, S. Louis, USA) was dissolved in 0.1 M phosphate-buffered saline (PBS, pH 7.4) and injected into the right basolateral amygdala in freely moving mice using a needle protruding 4.1 mm below the implanted cannula in order to evoke convulsive status epilepticus (SE) (Iori et al., 2017). SE was defined by the appearance of continuous spike activity with a frequency > 1 Hz intermixed with high amplitude and high frequency discharges lasting for at least 5 s, with a frequency of > 8 Hz. Spikes were defined as sharp waves with amplitude at least 2.5-fold higher than the standard deviation of baseline and duration < 100 ms, or as a spike-and-wave with duration < 200 ms. SE developed after approximately 10 min post-KA injection, as previously described (Iori et al., 2017). Thereafter, 40 min from SE onset, mice were injected with diazepam (10 mg/kg, intraperitoneally, i.p.) to improve their survival by suppressing motor seizures, although EEG SE was not interrupted. After SE induction mice were recorded continuously (24/7) for 24 h. The end of SE was defined by the occurrence of inter-spike intervals longer than 1 s. Digitized EEG data were processed using the twin record and review software. SE duration and spiking activity were quantified using clampfit 10.7 program (Axon Instruments, Perth, Australia).

2.4. Spontaneous seizures detection and quantification

Epilepsy development after SE in this model was described in detail before (Di Nunzio et al., 2021; Frigerio et al., 2018b; Iori et al., 2017). To study epilepsy development, mice were EEG recorded continuously (24/7) for 14 days, starting from SE induction, after baseline recording was done. Epilepsy onset was defined by the occurrence of two spontaneous seizures at least 48 h after the end of SE to differentiate spontaneous from acute symptomatic seizures. Fourteen days post-SE, mice were temporarily disconnected from the EEG set up, and left in their home cage until they were again EEG monitored (24/7) at 2.0 months post-SE for 2 weeks, corresponding to the chronic epilepsy phase. Spontaneous seizures are EEG ictal events characterised by high frequency (>5 Hz, usually 7–10 Hz) and/or multispike complexes and/or high amplitude (700 μV–1.0 mV vs 100–300 μV at baseline) synchronized spikes lasting 30–60 s on average occurring in both hemispheres, and accompanied by generalized motor convulsions (Suppl. Fig. 1A) (Di Nunzio et al., 2021; Frigerio et al., 2018b; Iori et al., 2017). In this study, mice undergoing epilepsy were not video-monitored therefore the treatment effect was assessed by counting EEG seizures.

In each mouse, we measured the total number of EEG seizures during the recording period under evaluation and the average seizure duration (the total time spent in seizures divided by the total number of seizures). In the experiment where mice were treated with reparixin or its vehicle during early disease development (for 6 days since SE induction), seizure number was compared in the same recording period between the two experimental groups. In the experiment where mice were treated with reparixin or vehicle in the chronic epilepsy phase (from 2.0 to 2.5 months post-SE), number of seizures during 2 week-drug treatment or vehicle was compared with the corresponding 2 week-pre-treatment baseline in each mouse (from 1.5 to 2.0 months). We also compared the % difference in the number of seizures (seizure number during treatment or vehicle *minus* seizure number during respective baseline/seizure number during baseline x100) in the reparixin-treated group vs the vehicle-treated group. The statistical tests used to analyze the data are reported in the respective legends.

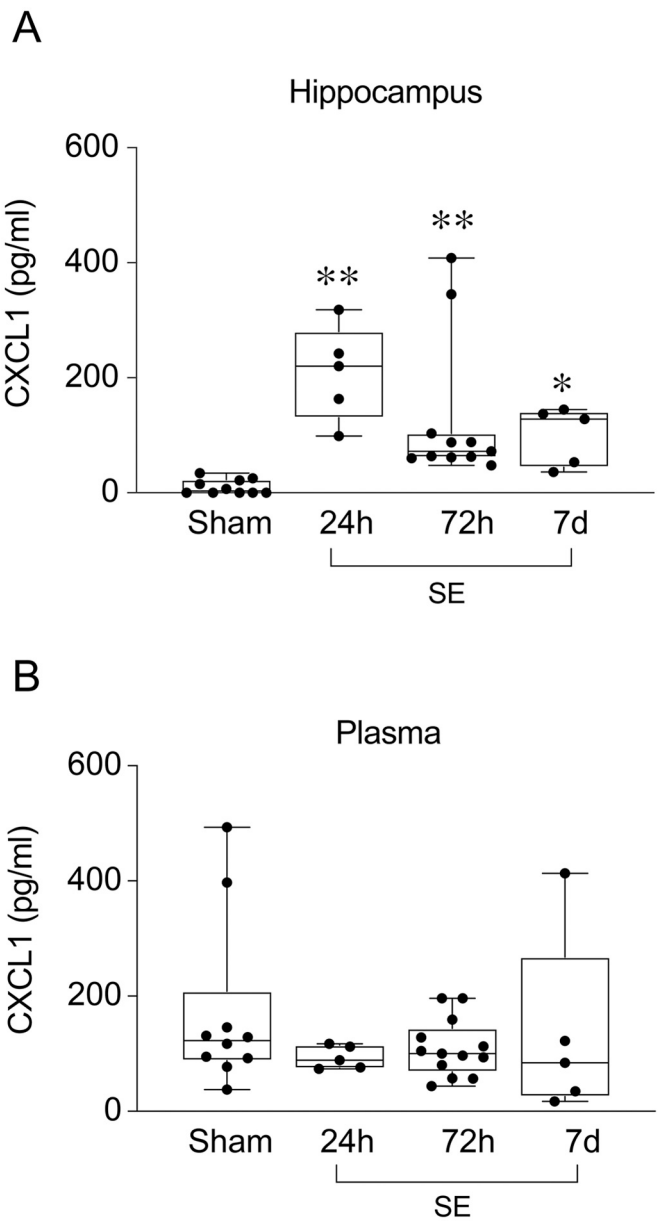

Fig. 1. Brain and plasma levels of CXCL1 after status epilepticus.
Panels A,B depict the concentration of CXCL1 in the hippocampus (A) and plasma (B) in sham mice ($n = 10$) and in status epilepticus (SE)-exposed mice that were killed 24 h, 72 h and 7 days after SE onset ($n = 5$–13). Two mouse hippocampi at 72 h were improperly dissected out therefore they were not included in the assay. Data are presented as box-and-whisker plots depicting median, minimum and maximum, and single values. $^{*}p < 0.05$, $^{**}p < 0.01$ vs sham by Kruskall-Wallis test followed by Dunn's post-hoc test.

2.5. Minipump implantation for reparixin administration

Previous pharmacological studies have demonstrated that treatment by continuous infusion is the optimal route of administration for reparixin, and the dose 7.5 mg/h/kg reduced pathologic outcomes in preclinical models of liver ischemia and neuropathic pain (Brandolini et al., 2017; Cavalieri et al., 2005).

For this reason, minipumps (Alzet pump 1007D, 100 Ml/minipump, 0.5MI/h or Alzet pump 2002, 200 Ml/minipump; 0.5 μl/h; Charles River, Calco, VA, Italy) were filled with reparixin (7.5 mg/h/kg; dissolved in sterile saline) or its vehicle (sterile saline) using a sterile syringe, then kept for 12 h at 37 °C before implantation, according to the manufacturer's instructions. Mice were implanted subcutaneously with

minipumps under general gas anaesthesia (1–3% isoflurane in O_2) by making a small incision between the scapulae and forming a subcutaneous pocket by gently spreading apart the connective tissue. The pump was inserted into the pocket with the flow moderator pointing away from the incision. Finally, the skin was carefully sutured to avoid any discomfort to the animal. Upon awakening from anaesthesia, mice were returned to their home cages. The procedure was completed in about 10 min.

Reparixin or vehicle was infused for 24 h before SE and for 3 days (Suppl. Fig. 2) or 6 days after SE (Fig. 3 and Suppl. Fig. 4), or for 14 days in chronic epileptic mice (Fig. 4). Plasma levels of reparixin were measured in mice at the end of drug infusion (i.e., after 7 days infusion in mice depicted in Suppl. Fig. 4; after 14 days infusion in mice depicted in Fig. 4).

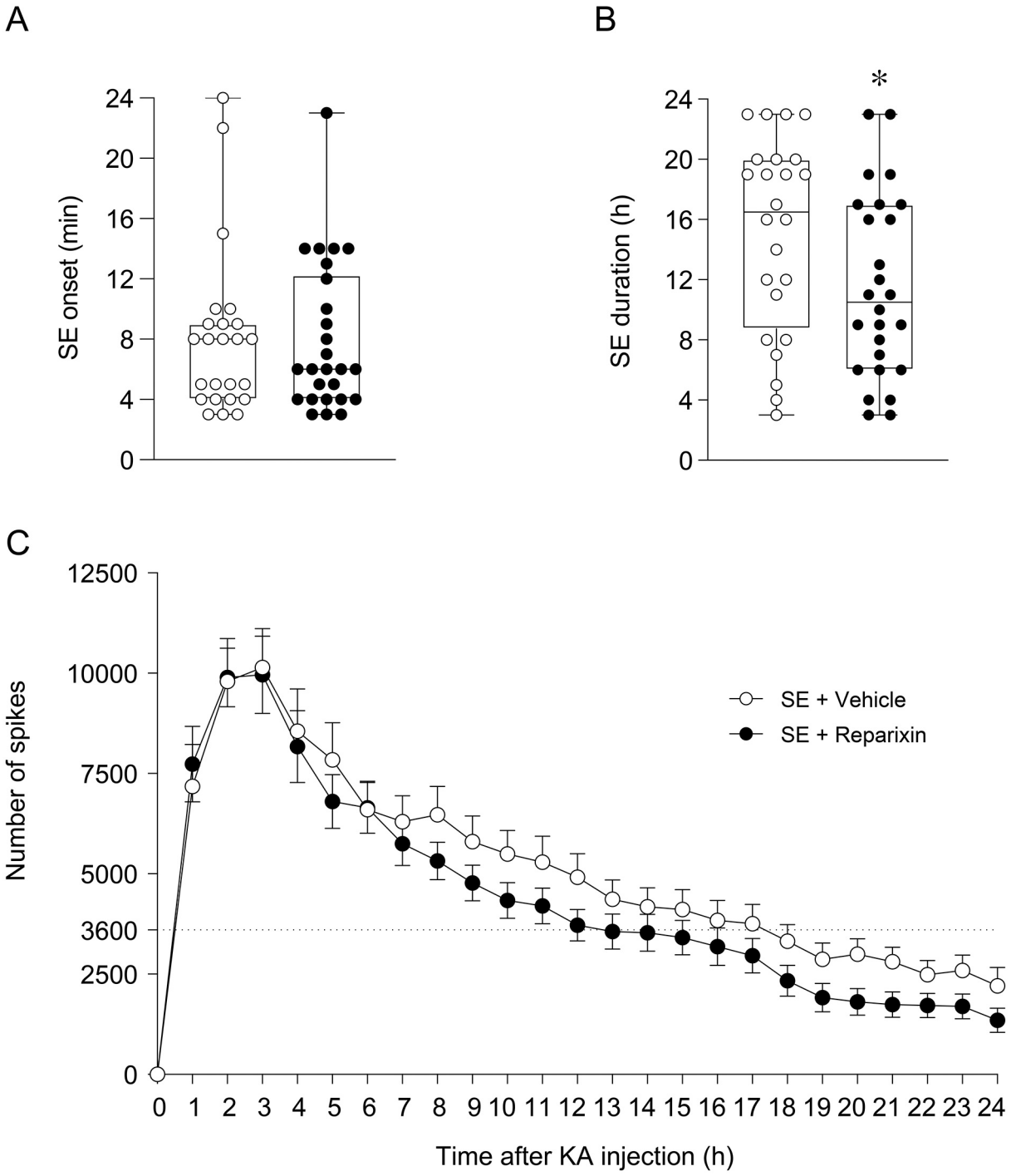

Fig. 2. Effect of reparixin on status epilepticus.

Panels A, B: SE onset (A) and total duration (B) in mice treated with reparixin ($n = 26$) or its vehicle ($n = 24$). Data are from mice depicted in Fig. 3 and Suppl. Figs. 2 and 4, and are presented as box-and-whisker plots depicting median, minimum and maximum, and single values. *$p < 0.05$ vs SE + Vehicle by two-tailed Mann-Whitney *U* test.

Panel C shows the temporal spike distribution during SE in the two experimental groups. Each point represents the cumulative number of spikes during progressive 1 h intervals. The dotted line represents the threshold number of spikes/h (3.600) below which SE elapses (inter-spike intervals >1 s). Data are presented as mean ± SEM.

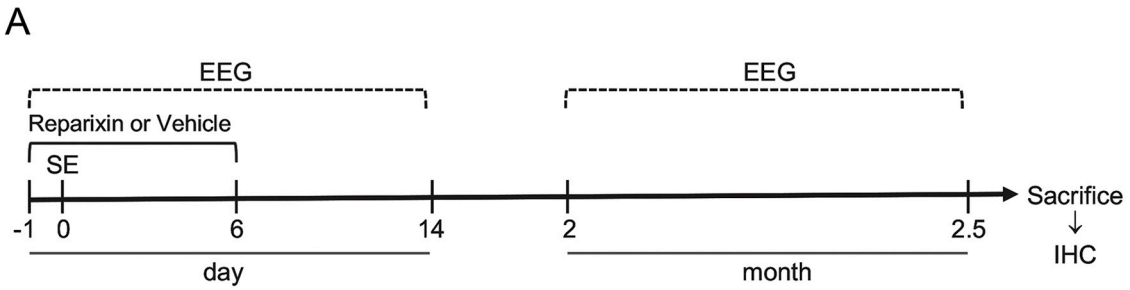

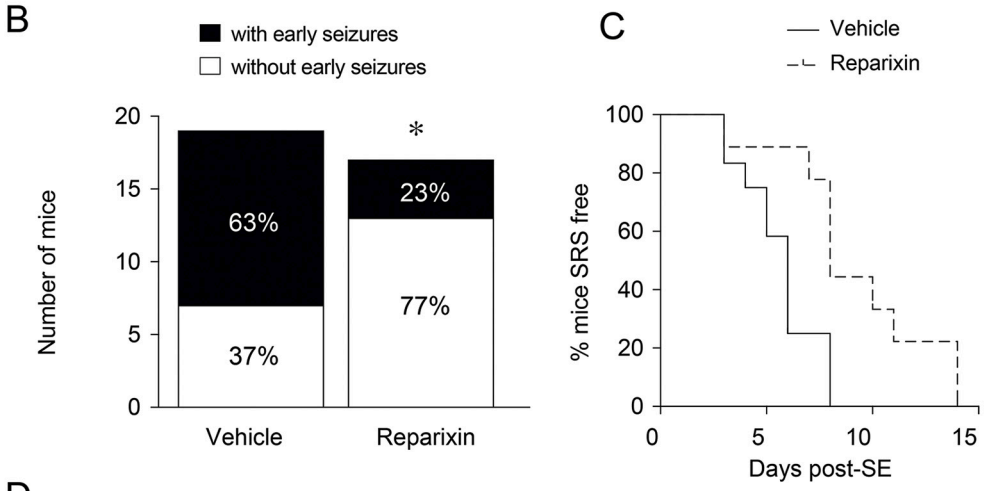

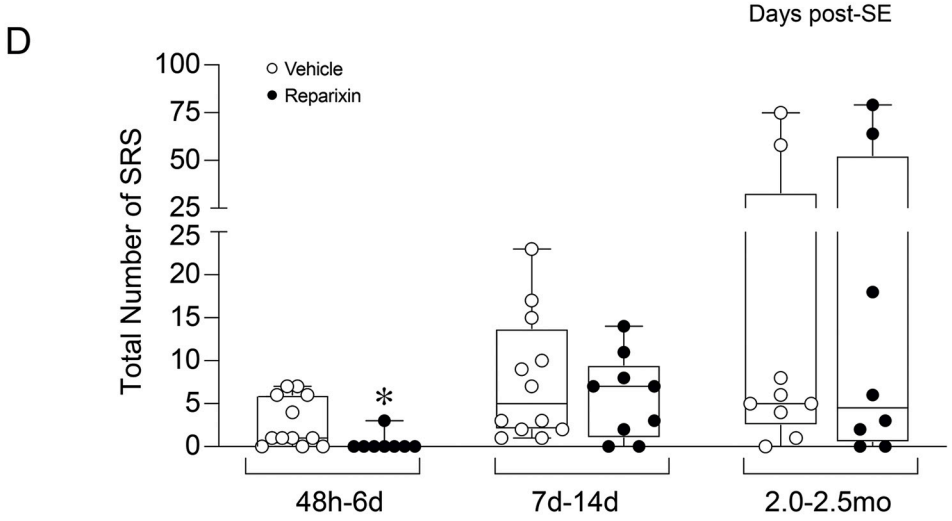

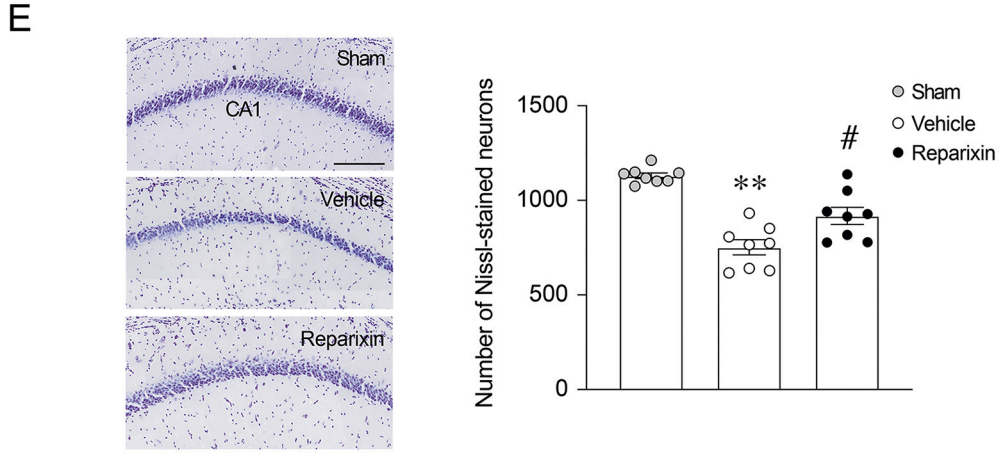

(caption on next page)

Fig. 3. Effect of reparixin on epilepsy development.
Panel A depicts the experimental protocol of the longitudinal study.
Panel B: bargrams depict the incidence of early seizures (intermixed with epileptiform spikes) during 48 h post-SE in vehicle- ($n = 19$) and reparixin-treated mice ($n = 17$). *$p < 0.05$ vs vehicle by Fisher's exact test.
Panel C: Kaplan-Meier survival curve reporting the percentage of mice developing the first spontaneous seizure as a function of days after SE in the two experimental groups ($n = 9$–12/group). $p < 0.05$ by Log-rank test.
Panel D depicts the total number of spontaneous seizures in three subsequent phases of disease development post-SE: 2–6 days (treatment or vehicle period); 7–14 days (drug wash-out period); 2.0–2.5 months (chronic epilepsy phase). Three vehicle and 1 reparixin mice died between 2.0 and 2.5 months post-SE therefore seizures were counted in these mice only in the preceding epochs. Data are presented as box-and-whisker plots depicting median, minimum and maximum, and single values. *$p < 0.05$ during 2–6 days post-SE vs vehicle by two-sided binomial test followed by Bonferroni post-hoc test.
Panel E depicts representative photomicrographs of Nissl-stained CA1 pyramidal neurons in chronic epileptic mice treated with vehicle or reparixin during epileptogenesis (*same mice of panel D*), and in sham mice. Mice were killed at the end of EEG monitoring (*protocol in panel A*). Scale bar: 200 μm. Quantitative analysis is reported in bargrams ($n = 8$ each group). One mouse was discarded in the vehicle group because of poor quality of Nissl staining which precluded a sound quantification of neuron number. Data are presented as mean ± SEM, and single values. **$p < 0.01$ vs sham by one-way ANOVA followed by Tukey's post-hoc test; #$p < 0.05$ vs vehicle by two-tailed *t*-test.

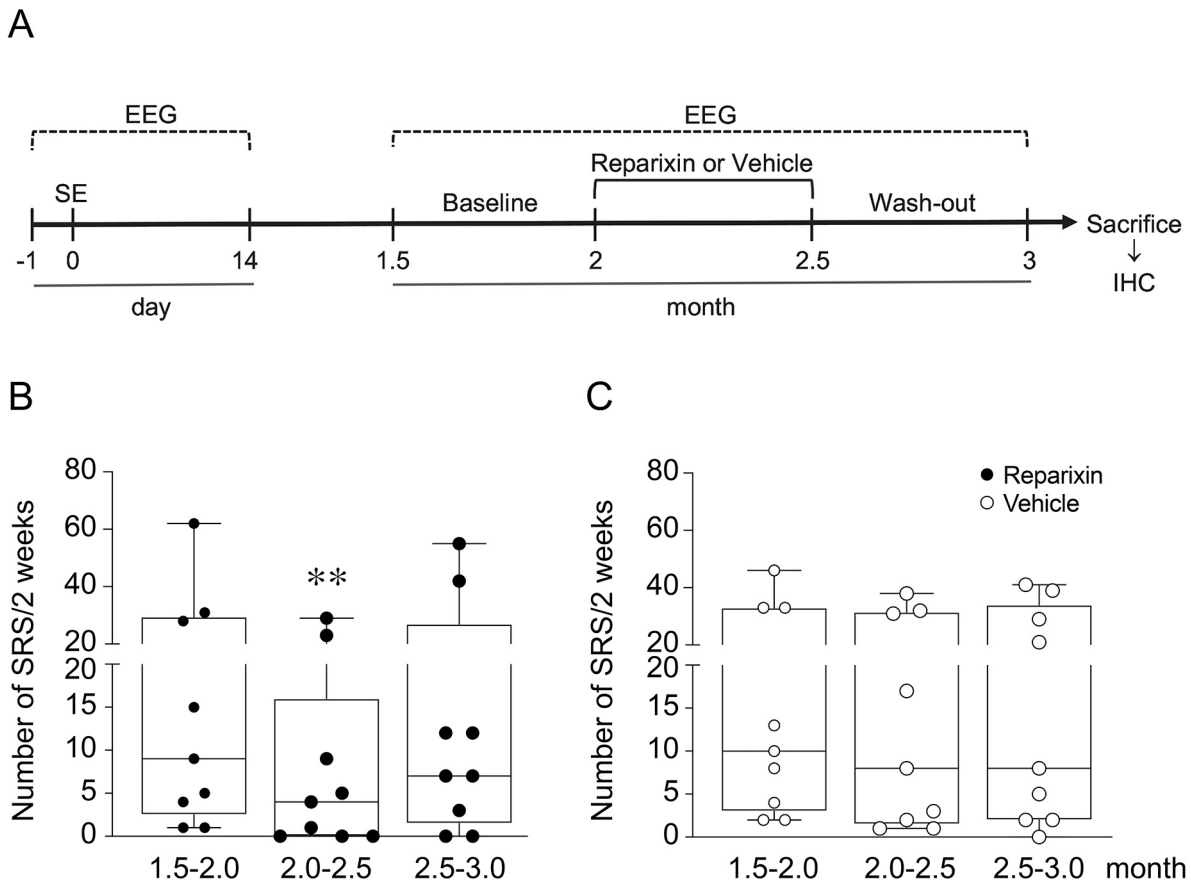

Fig. 4. Effect of reparixin on spontaneous seizures in epileptic mice.
Panel A depicts the experimental protocol applied in the study. Panels B, C depict the total number of spontaneous seizures in 3 subsequent monitoring phases post-SE in reparixin (B) or vehicle (C) treated groups (n = 9 each group): month 1.5–2.0 (baseline), 2.0–2.5 (treatment or vehicle period), 2.5–3.0 (drug discontinuation). Data are presented as box-and-whisker plots depicting median, minimum and maximum, and single values. **$p < 0.01$ vs respective pre-treatment baseline (month 1.5–2.0) by Friedman test followed by Dunn's post-hoc test. Reparixin reduced the number of seizures by 63 ± 13% vs respective baseline (B) compared to 24 ± 10% seizure reduction in vehicle-treated mice (C) ($p < 0.05$ vs vehicle group by two-tailed Mann Whitney U test).

2.6. Determination of reparixin in plasma samples

Blood was withdrawn from retromandibular plexus of lightly restrained mice using a needle (18 gauge) and collected in test tubes (K2 heparinized BD Microtainer tubes, 500 μl; Eysins, Switzerland). Plasma was obtained from heparinized blood by centrifugation at 1300 x*g* for 10 min at 4 °C and stored at −80 °C until analysis. The determination of reparixin levels in plasma samples involved a protein precipitation by acetonitrile (Sigma-Aldrich, S. Louis, MO, USA) addition (ratio 1:3). Samples were then centrifuged (20,000 x*g* for 15 min at 4 °C) and the supernatants were analyzed by a high-performance liquid chromatography (HPLC, Dionex-Thermo Fisher Scientific, Sunnivale, CA, USA) coupled with a mass spectrometer (MS, Thermofisher) equipped with an electrospray ionization (ESI) source for the detection. The chromatographic column was a Gemini C18 100 × 2.0 mm ID, 5 μ (Phenomenex, Torrance, CA, USA) and the lower limit of quantification was 0.05 μg/ml.

2.7. Immunohistochemistry and histological evaluation of cell loss in mice

2.7.1. Brain tissue preparation for histological analysis

Mice were deeply anesthetized (10% ketamine +10% medetomidine +80% saline; 10 ml/kg, i.p.) and perfused intracardially with 50 mM ice-cold phosphate buffered saline (PBS, pH 7.4) followed by 4% paraformaldehyde (PFA) in PBS. Brains were removed from the skull and post-fixed for 90 min in 4% PFA in PBS at 4 °C, transferred in 20% sucrose in PBS for 24 h at 4 °C, then frozen in n-pentane for 3 min at −50 °C, and stored at −80 °C until assay.

Serial coronal sections (−1.34 to −1.58 mm *from bregma*) (Franklin and Paxinos, 2008) were cut on a cryostat throughout the septal extension of the hippocampus. Quantitative analyses were performed in the septal hippocampus ipsilateral to the injected amygdala since the histopathology is mainly restricted to the injected hemisphere (*our unpublished observations*, and Mouri et al., 2008). Mice undergoing chronic EEG monitoring and used for the quantification of neuronal cell loss and CXCL1-CXCR1/2 immunostaining were electrode-implanted in the contralateral hippocampus therefore we could not perform histological analysis in corresponding slices. Slices at the same antero-posterior levels were matched for each control and experimental mouse.

*Nissl staining (mice of*Fig. 3*).* One slice every 4 coronal sections was stained with cresyl violet. Cell loss was quantified as previously described using 3 slices for each area of interest (Di Nunzio et al., 2021). Briefly, images of the septal pole of the hippocampus were captured at 20× magnification using a Virtual Slide scanning microscopy system (Olympus, Germany) and images were digitized. Neuronal cell loss was quantified by manually counting the number of Nissl-stained neurons in CA1 and CA3/CA4 pyramidal cell layers, and the hilar interneurons. We previously compared this method of quantification with stereological cell counting (Pascente et al., 2016). This comparative analysis showed that the extent of neuronal cell loss in the hippocampus of epileptic animals was similarly determined by the two methods of quantification.

*Fluoro-Jade (mice of*Suppl. Fig. 2*; data reported in main text).* Labeling was carried out as previously described (Terrone et al., 2018). Briefly, 3 slices/mouse brain were dried in ethanol (100%, 75% and 50%) and rehydrated in distilled water. Then, they were incubated in 0.06% potassium permanganate, washed in distilled water and transferred to 0.001% Fluoro-Jade staining solution. Sections were then rinsed in distilled water, mounted onto gelatin-coated slides, dried, immersed in xylene and coverslipped.

*Acetylated-α-tubulin (mice of*Suppl. Fig. 2*).* Slices (3/mouse brain) were blocked for 30 min at 4 °C in blocking buffer (0.1% Triton-X100, 3% BSA in PBS) then incubated with primary antibody against acetylated α-tubulin (mouse monoclononal Ab; Abcam, Cambridge, MA, USA; 1:2000) overnight at 4 °C. After washing with PBS, slices were incubated with secondary antibody (Alexa Fluor 488 anti-rabbit polyclonal Ab;

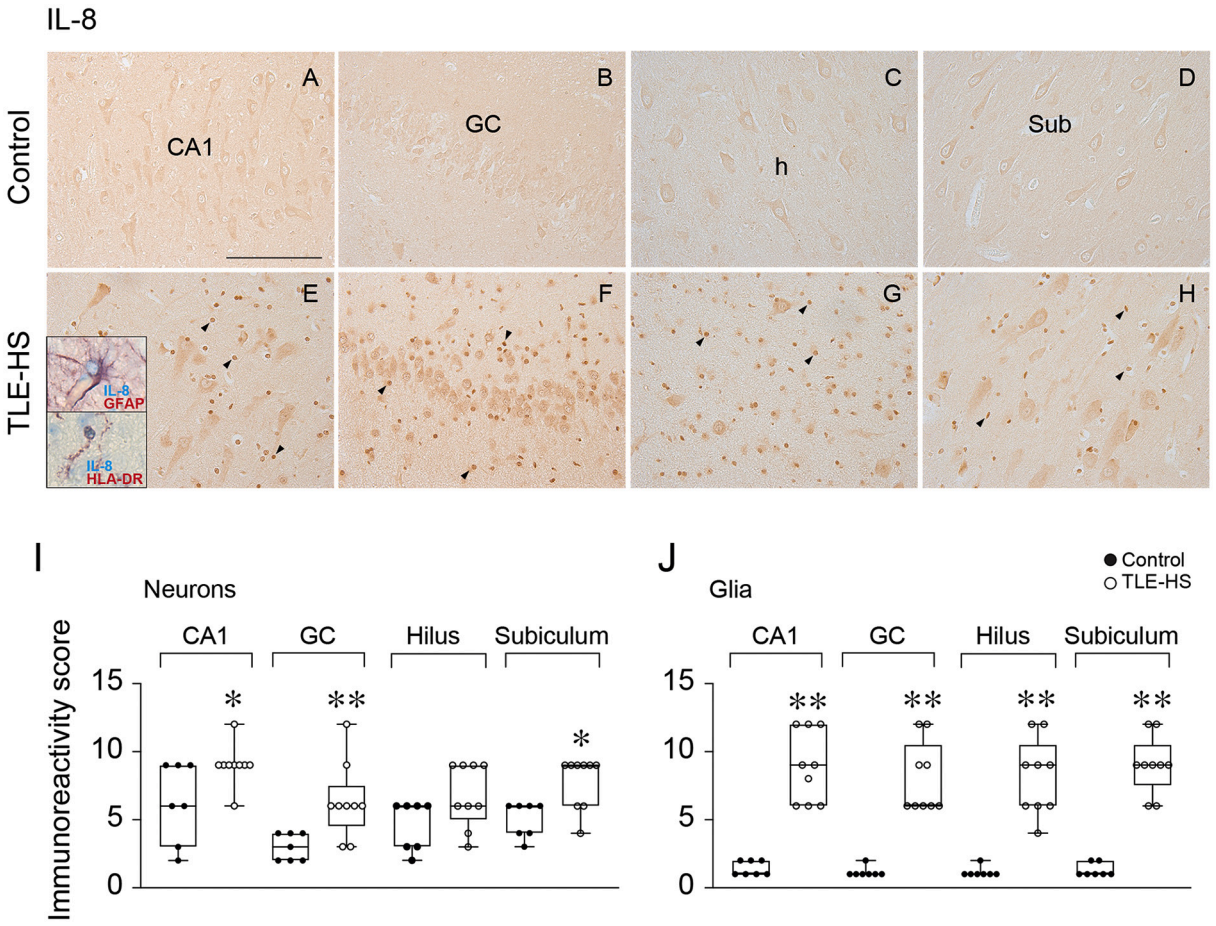

Fig. 5. IL-8 expression in patients with temporal lobe epilepsy and hippocampal sclerosis.
Panels A-H depict representative immunohistochemical micrographs showing the expression of IL-8 in the hippocampal formation of control (A-D) and temporal lobe epilepsy with hippocampal sclerosis (TLE-HS; E-H) specimens. CA1 pyramidal cell layer (A,E), granule cell layer (GC; B,F), hilus (h; C,G) and subiculum (D,H). Arrowheads show IL-8-immunoreactive glial cells. Insets in E show IL-8-positive microglia (co-localization with HLA-DR) and astrocyte (colocalization with GFAP). Scale bar: 75 μm; insets 3× magnification.
Bargrams (I,J) show semi-quantitative analysis of IL-8 immunoreactivity in neurons (I) and glia (J) in control ($n = 7$) and TLE-HS (n = 9). Data are presented as box-and-whisker plots depicting median, minimum and maximum, and single values. *$p < 0.05$, **$p < 0.01$ vs respective control by two-tailed Mann-Whitney U test.

Jackson Immunoresearch Laboratories, Inc., USA; 1:500) for 1 h at room temperature and mounted on slides with fluorescein mounting medium (Vectashield, Vector Labs, Burlingame, CA, USA).

*CD45 (same mice of*Suppl. Fig. 2*; data reported in the main text)*. Slices (2/mouse brain) were incubated overnight at 4 °C with a primary anti-CD45 biotinylated antibody (mouse monoclonal Ab; BD Pharmingen, San Jose, CA, USA; 1:500) in 3% FBS in 0.1% Triton X-100 in PBS. Immunoreactivity was tested by avidin–biotin–peroxidase (Vector Labs, USA). Sections were stained using diaminobenzidine. At the end of immunohistochemical procedures, slices were mounted onto gelatin-coated slides, dehydrated in graded alcohols, and coverslipped.

Data obtained in 2 or 3 slices/mouse brain were averaged, thus providing a single value for each mouse, and this value was used for statistical analysis.

*CXCL1, CXCR1/2 (*Suppl. Fig. 5*; same vehicle-injected epileptic mice of*Fig. 4*)*. Mice were deeply anesthetized (10% ketamine+10% medetomidine+80% saline; 10 ml/kg, i.p.) and perfused intracardially with 50 mM ice-cold PBS (pH 7.4). Brains were removed from the skull and post-fixed for 48 h in 10% formalin at 4 °C and subsequently embedded in paraffin. Paraffin-embedded tissue was sectioned at 5 μm, mounted on pre-coated glass slides and processed for immunohistochemical staining. Sections (3 slices/mouse) were dewaxed in xylene, rinsed in ethanol (100%, 95%, 70%) and incubated for 20 min in 0.3% hydrogen peroxide diluted in methanol to block endogenous peroxidase activity. Antigen retrieval was performed using a microwave (3 cycles of 5 min each at 750 W) in Tris+EDTA buffer (pH 9.0). Slides were washed with PBS and incubated overnight with primary antibody against CXCL1 (rabbit polyclonal Ab; Bioss Antibodies, Woburn, MA, USA; 1:250), or CXCR1 (rabbit polyclonal Ab; Invitrogen, Waltham, MA, USA; 1:300), or CXCR2 (rabbit polyclonal Ab; Abcam, Cambridge, MA, USA; 1:500) in PBS and 10% normal goat serum at 4 °C. CXCL1 antibody cross-reacts only with mouse and rat tissues, while CXCR1 and CXCR2 antibodies cross-react with human, mouse and rat. Different antibodies were used in human tissue (*see below*). CXCL1 antibody was previously used to detect the chemokine in paraffin-embedded mouse tissue sections (Ito et al., 2017). For CXCR1 and CXCR2 antibodies, the datasheets provided images of specific immunostaining in paraffin-embedded mouse tissue. Immunoreactivity was tested by avidin–biotin–peroxidase. Sections were stained using diaminobenzidine, counterstained with hematoxylin, dehydrated in alcohol and xylene and coverslipped.

In all immunohistochemical analyses, tissue was also incubated with antibody diluent alone or without the specific primary antibody to serve as negative control, and essentially no staining was observed.

2.8. ELISA

For CXCL1 measurements (Fig. 1), brains were harvested after rapid (2 min) intracardiac perfusion with 50 mM ice-cold PBS (pH 7.4) in mice that were deeply anesthetized (10% ketamine +10% medetomidine +80% saline; 10 mL/kg, i.p.) Then, hippocampi from both hemispheres were dissected out at 4 °C, immediately frozen in liquid nitrogen and stored at −80 °C until assay. Blood was withdrawn from the heart atrium and transferred in Vacutainer test tubes kept on ice until centrifugation at 1300 *xg* for 10 min at 4 °C. After centrifugation, the supernatant (i.e., plasma) was collected and stored at −80 °C until assay.

Hippocampi of the injected hemisphere were homogenized (100 mg/500 μl) on ice in a test tube containing PBS and protease inhibitors (5 μg/ml leupeptin, pepstatin, chimostatin, aprotinin and 1 mM PMSF; Sigma-Aldrich, St Louis, MO, USA). Then samples were centrifuged at 13645 rpm at 4 °C for 15 min (Centrifuge 5417 R, Eppendorf). Supernatants were collected and stored at −80 °C until use. CXCL1 was measured using mouse CXCL1/KC ELISA kit (R&D Systems, Minneapolis, MN, USA), according to manufacturer's instructions. The optical density (OD) of the multi-well was measured within 30 min after the STOP solution by using a Tecan (infinite m200 pro) reader at the wavelength of 450 nm. The calibration curve generated was used to extrapolate the CXCL1 concentration in the samples.

For MMP9 measurement, blood was collected from retromandibular plexus in SST tubes (BD Microtainer, 500 μl) before sacrifice at the end of EEG monitoring (*same mice of* Fig. 4) and serum was isolated by centrifugation at 15000 *xg* for 2 min at room temperature and stored at −80 °C until assay. MMP9 was determined in duplicate/mouse using AlphaLisa MMP9 mouse kit (Perkin Elmer, Waltham, MA, USA), according to Pasetto et al. (2017). The average value from each duplicate/mouse was expressed in pg/ml and used for the statistical analysis.

2.9. Western blot

Brains were harvested from deeply anesthetized mice (Suppl. Figs. 3 and 4) (10% ketamine +10% medetomidine +80% saline; 10 mL/kg, i.p.) after rapid (2 min) intracardiac perfusion with 50 mM ice-cold PBS (pH 7.4). Subsequently, hippocampi of both hemispheres were dissected out on ice and immediately frozen in liquid nitrogen, and stored at −80 °C until assay. The hippocampus of the injected hemisphere was homogenized (30 mg/150 μl) at 4 °C in 20 mM Tris-HCl (pH 7.4), 5 mM EGTA, 1 mM EDTA, 1 mM Na-orthovanadate with protease and phosphatase inhibitor cocktail (Sigma-Aldrich, St Louis, MO, USA). Protein concentration of lysates were quantified with a BCA protein assay kit (Pierce Biotechnology, Rockford, IL, USA): 30 μg protein of each sample were run in duplicate on a 10% acrylamide SDS-PAGE gel using electrophoresis and transferred to a nitrocellulose membrane. For western blot analysis, we used antibodies against Kir4.1 (rabbit polyclonal Ab; Alamone Laboratories, Jerusalem, Israel; 1:2000), GLT-1 (rat monoclononal Ab; Abcam, Cambridge, MA, USA; 1:1000), GFAP (mouse monoclonal Ab; Chemicon Int. Inc., Temecula, CA, USA; 1:10000), and actin (mouse monoclonal Ab; Chemicon Int. Inc.; 1:5000). The hippocampus of the contralateral hemisphere was used to measure albumin (rabbit polyclonal Ab; Dako, Santa Clara, CA, USA; 1:10000) in brain parenchyma, as index of BBB damage. The membranes were probed with horseradish peroxidase-conjugated secondary antibody. Immunoreactivity was visualized with enhanced chemiluminescence (BIO-RAD, Hercules, CA, USA). The band optical density was acquired by Chem-iDoc imaging system (BIO-RAD) and quantified by Image lab software 6.0 (BIO-RAD). GFAP and actin proteins were used as a loading control to normalize the relevant protein bands. The values from two replicates/each hippocampus were averaged, thus providing a single value for each mouse, and this value was used for the statistical analysis.

2.10. Immunohistochemistry and signal quantification in human tissue

The surgical and post-mortem brain tissue included in this study was obtained from the archives of the Department of Neuropathology of the Amsterdam UMC, (Amsterdam, The Netherlands). Hippocampal brain biopsies were obtained from patients undergoing surgery for intractable epilepsy and diagnosed with TLE (Figs. 5 and 6, Suppl Figs. 6 and 7). All cases were reviewed independently by two neuropathologists. The classification of hippocampal sclerosis (HS) was determined as described by the International League Against Epilepsy (Blumcke et al., 2013) (TLE-HS: $n = 7$–9; TLE-no-HS: $n = 6$). The hippocampus of age-matched controls ($n = 5$–7) without a history of seizures or other neurological diseases was obtained at autopsy within 24 h after death. While we acknowledge the limitation of the use of autopsy material, it represents the only readily available source of brain tissue unaffected by neurological diseases. Additionally, we analyzed surgical TLE-no HS tissue to distinguish the contribution of epileptic seizures vs histopathological changes. Clinical details of patient cohorts and number of samples for experiments used in this study are summarized in Suppl. Table 1. Tissue was obtained with informed consent for the use in research and access to medical records in accordance with the Declaration of Helsinki and the Amsterdam UMC Research Code provided by the Medical Ethics Committee.

Human brain tissue was fixed in 10% buffered formalin and

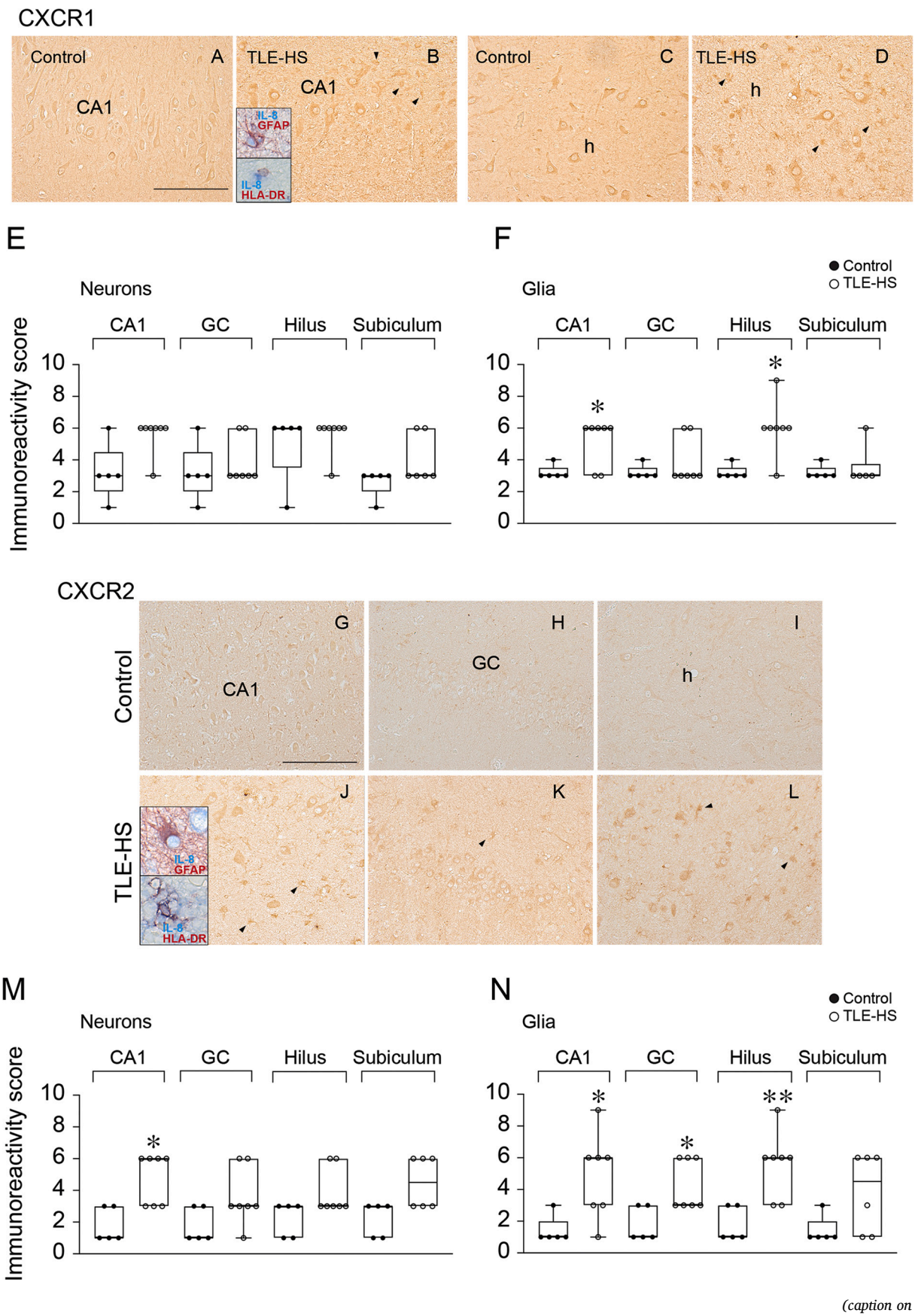

(caption on next page)

Fig. 6. CXCR1 and CXCR2 expression in patients with temporal lobe epilepsy and hippocampal sclerosis.
Panels A-D depict representative immunohistochemical micrographs showing the expression of CXCR1 in CA1 and the hilus (h) of a control (A,C) and temporal lobe epilepsy patient with hippocampal sclerosis (TLE-HS) (B,D). Arrowheads depict representative CXCR1-immunoreacrive glial cells. Insets in B show CXCR1-positive astrocyte (co-localization with GFAP) and microglia (co-localization with HLA-DR). Scale bar: 75 μm; insets 3× magnification.
Panels G-L depict the expression of CXCR2 in the hippocampus from control (G-I) and TLE-HS (J-L). CA1 pyramidal cell layer (G,J), granule cell layer (GC; H,K) and hilus (I,L). Arrowheads depict representative CXCR2-immunoreactive glial cells. Insets in J show CXCR2-positive astrocyte (co-localization with GFAP) and microglia (co-localization with HLA-DR). Scale bar: (A,G) 75 μm; insets 3× magnification.
Bargrams in E,F and M,N show the semi-quantitative analysis of CXCR1 and CXCR2 immunoreactivity, respectively, in neurons (E,M) and glia (F,N) in control (n = 7) and TLE-HS specimens (n = 9). Data are presented as box-and-whisker plots depicting median, minimum and maximum, and single values. *$p < 0.05$, **$p < 0.01$ vs respective control by two-tailed Mann-Whitney U test.

embedded in paraffin. Paraffin-embedded tissue was sectioned at 6 μm and mounted on pre-coated glass slides (Star Frost, Waldemar Knittel Glasbearbeitungs, Braunschweig, Germany). Sections (one section/patient/marker) were dewaxed in xylene, rinsed in ethanol (100%, 95%) and incubated for 20 min in 0.3% H_2O_2 in methanol to block endogenous peroxidase activity. Antigen retrieval was performed using a pressure cooker in 0.01 M sodium citrate buffer (pH 6.0) at 121 °C for 10 min. Slides were washed with phosphate buffered saline (PBS; 0.1 M, pH 7.4) and incubated overnight with primary antibodies against IL-8 (rabbit polyclonal Ab; Abcam, Cambridge, UK; 1:50), CXCR1 (mouse monoclonal Ab, clone #42705; R&D systems, Minneapolis, MN, USA; 1:100) and CXCR2 (mouse monoclonal Ab, clone #48311; R&D systems, Minneapolis, MN, USA; 1:100) at 4 °C. Thereafter, slides were washed in PBS and visualized with a polymer-based horse radish peroxidase (HRP) immunohistochemistry detection kit (Brightvision plus kit, ImmunoLogic, Duiven, The Netherlands) according to the manufacturer's instructions. After washing in PBS, sections were stained using 3,3′-diaminobenzidine (DAB) tetrahydrochloride (Sigma-Aldrich, St. Louis, MO, USA) with 0.015% H_2O_2 in 0.05 M Tris-HCl buffer (pH 7.6). Colour development was stopped by washing in distilled water. Sections were counterstained with Hematoxylin-Mayer solution (Klinipath, Breda, The Netherlands), washed with tap water, dehydrated in alcohol and xylene and coverslipped in Pertex (VWR International, Radnor, PA, USA).

IL-8 and CXCR1/2 antibodies cross-react only with human specimens, as detailed on manufacturer's datasheets. The IL-8 antibody was previously used to detect the chemokine in paraffin-embedded human tissue sections (Raja et al., 2017). Moreover, using this antibody, we also detected IL-8 immunoreactivity in the leptomeninges and in capillaries in cells with macrophage morphology, according to the expected expression pattern of IL-8. CXCR1 and CXCR2 monoclonal antibodies have been rigorously validated without cross-reactivity for each other, as detailed in the manufacturer's data sheet. Tissue incubated with antibody diluent alone or without the primary antibody served as negative control and was essentially blank.

Double-labelling was performed with glial fibrillary acidic protein (GFAP; mouse monoclonal Ab, clone GA5; Sigma-Aldrich, St. Louis, MO, USA; 1:4000) or HLA-DP/DR/DQ (HLA-II, mouse monoclonal Ab, clone CR3/43; Agilent, Santa Clara, CA, USA; 1:100). Sections were incubated overnight with primary antibody (IL-8/CXCR1) and the next day incubated with BrightVision poly-HRP anti-rabbit (Immunologic, Duiven, The Netherlands) for 30 min at room temperature and washed with PBS. Staining was developed using 3′-amino 9′-ethylcarbazole (AEC, Sigma-Aldrich, St. Louis, MO, USA) in 0.05 M Acetate buffer with 0.5% H_2O_2 filtered substrate solution. To remove the first primary antibody, sections were cooked in citrate buffer and then washed with PBS. Incubation with the second primary antibody was performed overnight followed by incubation with poly-alkaline phosphatase (AP)-anti-rabbit (Immunologic, Duiven, The Netherlands) for 30 min at room temperature the next day. AP activity was visualized with the AP substrate kit III Vector Blue (SK-5300, Vector Laboratories Inc., Burlingame, CA, USA). Sections incubated without the primary antibody were essentially blank. Finally, stained sections were air dried and coverslipped using VectaMount (Vector Labs, Burlingame, CA, USA).

Quantification of immunohistochemistry. Semi-quantitative analysis of surgically resected tissue was performed as described previously (Arena et al., 2019). Briefly, tissue sections were evaluated by two independent observers trained for histopathological evaluation of surgically resected tissue [including routine identification of anatomical subregions, discrimination of cell types (e.g., neurons vs glia), identification of histopathological abnormalities from epilepsies of various etiology, evaluation of intensity and distribution of staining using standard staining techniques] in the department of (neuro)pathology of the Amsterdam University Medical Centers. All samples underwent histopathological revision by a trained neuropathologist before the evaluation of the investigated markers.

Immunoreactivity (IR) was scored using a scale 0–3 (0 = absent, 1 = weak, 2 = moderate, 3 = strong staining) for CXCR1/CXCR2 and 0–4 (0 = absent, 1 = weak, 2 = moderate, 3 = strong, 4 = very strong staining) for IL-8. In the case of discordant evaluations, independent re-evaluation was performed by both observers to define the final score. Neurons and glia in the hippocampal subfields *cornu ammonis* 1 (CA1), granule cell layer (GC), hilus (h) and subiculum (Sub) were examined and the score represents the predominant intensity found in each case. In addition, the frequency of cells positive for the investigated markers was evaluated (0 = absent, 1 = low, 2 = moderate, 3 = high, 4 = very high). The product of intensity and frequency was used to obtain the overall IR score (Figs. 5 and 6, Suppl. Figs. 6 and 7).

2.11. Data analysis

In each experiment, simple randomization with 1:1 allocation ratio was applied to assign a subject to a particular experimental group using a website randomization program (www.randomization.com). Mice were randomized to drug or vehicle group before inducing SE or in naïve conditions, or in chronic epilepsy and the individual mouse represented the experimental unit. To take into account the potential loss of mice during the longitudinal experiment, we prospectively increased the number of animals by 25%, as indicated by previous experiments using this epilepsy model.

Statistical analysis was performed by GraphPad Prism 8 (GraphPad Software, USA) for Windows using raw data. Choice between parametric and non-parametric tests depended on passing the Shapiro-Wilk normality test. Data analyzed by non-parametric tests are presented as box-and-whisker plots depicting median, interquartile interval, minimum and maximum, and single values (n = number of individual mice or samples). Data analyzed by parametric tests are presented as mean ± SEM, and single values (Fig. 3**E** and Suppl. Figs. 3 and 4). In each experiment, statistical analysis of data is reported in the respective figure legends. Differences between groups were considered significant for values of $p < 0.05$.

Blinding was applied to treatment administration, outcome assessment and data analysis. Animal exclusion from analysis is detailed in the result section. The primary outcome measure in mice under treatment was the reduction in the number of seizures; the secondary outcome measure was neuroprotection. Sample size was a priori determined based on previous experience with this animal model.

3. Results

3.1. CXCL1 brain and blood levels in mice developing epilepsy

We first studied whether CXCL1 was increased in the mouse hippocampus, a key epileptogenic region in the murine model. Mice were killed at 24 h ($n = 5$), 72 h ($n = 13$) and 7 days (n = 5) after induction of SE to encompass the early phase of disease development (epilepsy onset occurs within 5–7 days, *see* Fig. 3C). Sham animals (implanted with electrodes and not exposed to SE, $n = 10$) were used as time-matched controls.

Fig. 1 (panel **A)** shows that hippocampal level of CXCL1 was significantly increased above sham values (undetectable in 7 out of 10 mice): the increase occurred within 24 h from SE onset ($p < 0.01$) and persisted for at least 7 days ($p < 0.05$). We found a positive correlation between SE duration and CXCL1 level at 24 h ($r = 1.0$; $p = 0.0167$ by Spearman two-tailed test).

Plasma level of CXCL1 was measured from blood withdrawn from the same mice at sacrifice, and it was unaltered (Fig. 1**B**), supporting clinical evidence that IL-8 increases predominantly in CSF of epilepsy patients (Kenney-Jung et al., 2016; Sakuma et al., 2014).

3.2. Blood level and pharmacodynamic measure of reparixin effect

Reparixin plasma level was measured in SE-exposed mice that were killed at the end of 7 day-treatment (to mimic treatment schedule of Fig. 3) or at the end of 14-day treatment in chronic epileptic mice (Fig. 4), and we found therapeutic drug concentrations (μg/ml; 7 days: SE + drug, 23.1 ± 4.2, n = 5; 14 days: Epileptic mice+drug: 15.1 ± 2.3, $n = 8$) in accordance with those obtained in previous pharmacokinetic and efficacy experiments. Similar levels were attained in sham control mice (μg/ml; 7 days: Sham+drug, 17.3 ± 2.2; n = 5).

In particular, reparixin, administered at the same dose and regimen as in the present study, significantly reduced neurotrophils infiltration and hepatocellular necrosis 24 h after reperfusion in a rat model of liver ischemia (Cavalieri et al., 2005). Since reparixin has a high affinity for serum albumin (protein binding at 30 μg/ml = 99.9%), 15–30 μg/ml total blood concentration was selected to assure a free drug concentration corresponding to 50–100 nM. This concentration exceeds reparixin IC_{50} (about 1 nM) as assessed in CXCL1-induced rodent chemotaxis assay, and other relevant in vitro models (Bertini et al., 2004). In the present study reparixin level in the brain were undetectable, likely due to the small amount of hippocampal tissue. However, previous biodistribution studies in healthy rodents showed that in the presence of 15–30 μg/ml circulating drug concentration, the drug fraction distributed in the brain tissue corresponds to 0.02% of the reparixin circulating concentration (*unpublished data*). Based on these data, pharmacologically relevant concentration of the unbound drug in the brain tissue (12–24 nM) should be reached in our experimental model.

In sham mice, reparixin infusion for 7 days did not affect cognitive performance in Barnes Maze or motor activity (*not shown*) denoting a safety profile, in accord with clinical evidence (Goldstein et al., 2020).

We examined a pharmacodynamic measure of reparixin's effect in the CNS as a read-out of effective drug concentrations following our treatment schedule. Previous evidence showed that reparixin was able to inhibit the increase of acetylated-α-tubulin, an intracellular marker of microtubule stabilization, induced in neuronal cells by a neurotoxin (Brandolini et al., 2017). Therefore, we measured the expression of acetylated-α-tubulin in drug- vs vehicle-treated mice. Suppl. Fig. 2**A** depicts increased acetylated-α-tubulin in the hippocampus of SE-exposed mice 72 h post-SE (n = 8), and reparixin prevented this increase ($n = 14$). Suppl. Fig. 2**B** reports the quantification of reparixin's effect in the various hippocampal subfields (CA1, CA3 and hilus; $^{*}p < 0.05$; $^{**}p < 0.01$ vs SE + vehicle).

Reparixin permeates an intact blood-brain barrier (BBB) to a limited extent, but still compatible with the achievement of pharmacologically effective concentrations in the brain tissue (12–24 nM). Additionally, reparixin afforded therapeutic actions after systemic administration in animal models of brain ischemia and breast cancer's brain metastasis that are conditions associated with a leaky BBB (Brandolini et al., 2015; Garau et al., 2005). In the present study, we provide evidence for a significant increase in BBB permeability in our epilepsy model which might further facilitate free reparixin entry into the brain (*see* Discussion). Suppl. Fig. 3 shows significant serum albumin brain extravasation, an index of BBB damage, as assessed by western blot in the mouse hippocampus at the various times post-SE encompassing the window of drug-treatment (up to 7 days post-SE) ($p < 0.01$ vs sham mice). We also determined serum levels of MMP9, another marker of BBB damage (Rüber et al., 2018), by ELISA in chronic epileptic mice (*same mice of* Fig. 4). We found that MMP9 level was significantly increased in epileptic mice (ng/ml; 255.3 ± 81.9, $n = 6$) vs sham controls (ng/ml; 115.71 ± 37.4, $n = 4$; $p < 0.05$ by two-tailed Mann-Whitney *U* test).

3.3. Reparixin effect on status epilepticus and acute neuronal injury

Drug administration was started before SE induction in consideration of the time required for pump activation and to reach steady-state drug plasma concentration necessary for therapeutic efficacy. Moreover, we aimed at preventing the effects due to the increase in CXCL1 which occurred within 24 h from SE onset.

We measured whether reparixin affected SE by measuring quantitative parameters during drug infusion (Fig. 2). The treatment did not affect SE onset time (**A**) but shortened by 27% on average the duration of SE as compared to vehicle-infused mice (**B**). In particular, SE decayed at 15.0 ± 1.3 h in vehicle ($n = 24$) vs 11.4 ± 1.2 h in reparixin-treated mice ($n = 26$; $p < 0.05$). The overall number of spikes in the two experimental groups did not significantly differ (**C**).

Next, we assessed the extent of acute neuronal injury induced by SE by analysing Fluoro-Jade (FJ) positive neurons 72 h post-SE (randomly chosen mice from those where acetylated-α-tubulin was analyzed). We found a significant reduction in the number of mice showing FJ-positive neurons in the CA1 pyramidal layer: SE + vehicle, 5/5 mice; SE + reparixin, 2/7 mice ($p < 0.05$ by Fisher's test).

We also detected a significant reduction of CD45-positive leukocytes in adjacent hippocampal slices (*number of cells*; SE + vehicle, 181.6 ± 31.1, $n = 5$; SE + reparixin, 47.9 ± 15.8, n = 6, $p < 0.01$ by two-tailed Mann-Whitney U test), underscoring that reparixin inhibited the chemotactic action of CXCL1 (Bertini et al., 2004). CD-45-positive cells were undetectable in sham mice (n = 6).

3.4. Effect of reparixin on epilepsy development

We set out to determine the role of CXCL1 in the development of spontaneous seizures by randomizing mice to reparixin (*7.5 mg/h/kg; n* = 12) or vehicle (n = 12) s.c. infusion for 7 days (prodromal phase of epilepsy onset), starting treatment 24 h before SE (Fig. 3**A**).

Three mice in the vehicle group and 4 mice in the reparixin group were withdrawn from data analysis, as follows: 1 reparixin-treated mouse died 3 days post-SE and 2 reparixin-treated mice were incorrectly dosed with the minipumps, therefore a total of 3 reparixin mice were omitted from the longitudinal study. Three vehicle and 1 reparixin mice died between day 60 and day 74 post-SE therefore seizures were counted in these mice only during the preceding epochs.

Fig. 3 shows the incidence of acute symptomatic seizures and epileptiform spikes (depicted in Suppl. Fig. 1**B**) occurring within 2 days from SE onset (**B**), the onset time of spontaneous seizures (**C**) and the number of spontaneous seizures EEG monitored during treatment (*2–6 days*, to exclude symptomatic seizures), after dug discontinuation (*7–14 days*), and in the chronic epilepsy phase (*2.0–2.5 months*), as assessed by 24/7 EEG monitoring (**D**). Panel **B** depicts a reduced incidence of acute symptomatic seizures in reparixin-treated mice (23% of mice) compared to vehicle mice (63% of mice) ($p < 0.05$ by Fisher test) during 2 days

post-SE. Kaplan-Meyer survival curve (**C**) reports the percentage of mice developing spontaneous seizures as a function of time: reparixin-treated mice displayed a significant delay in the onset of spontaneous seizures vs vehicle mice ($p < 0.05$, Log-rank test). Panel **D** shows the number of spontaneous seizures during three subsequent epochs of recording: reparixin-treated mice showed a significant reduction of spontaneous seizures vs vehicle during the treatment period (2–6 days post-SE; $p < 0.05$) whereas seizures were similar to vehicle-infused mice after reparixin discontinuation (7–14 days and 2.0–2.5 months).

Fig. 3**E** depicts neuronal cell loss in the CA1 region of vehicle vs reparixin-treated mice killed at the end of EEG monitoring (2.5 months post-SE). Data showed a 33% decrease in the number of CA1 pyramidal neurons in epileptic mice receiving vehicle ($n = 8$; one mouse was discarded because of poor Nissl staining) vs sham mice ($n = 8$; $p < 0.01$). Epileptic mice treated with reparixin during 6 days post-SE ($n = 8$) showed a number of CA1 pyramidal neurons similar to sham mice, and significantly higher than epileptic mice treated with vehicle ($p < 0.05$ vs vehicle). Neurodegeneration was similar between the vehicle and reparixin groups in CA3 (*number of cells*; sham, 540.1 ± 70.2, SE + vehicle, 401.1 ± 33.3*, reparixin+SE, 365.0 ± 30.3*, *$p < 0.01$ vs sham) and hilus (*number of cells*; sham, 45.6 ± 3.2; SE + vehicle, 31.2 ± 4.3*, reparixin+SE, 33.9 ± 5.8*, *$p < 0.01$ vs sham).

CXCL1 was recently shown to contribute to astrogliosis, and to decrease astrocytic GLT-1 mediated glutamate uptake, thus leading to enhanced excitability of pyramidal neurons and promoting acute seizures, and these effects were mediated by CXCR2 receptors (Liu et al., 2020). Since astrocytes are a key cell population involved in seizures (Devinsky et al., 2013), we explored whether reparixin's anti-seizure effect observed during the early disease phase (i.e., 6 days post-SE) was associated with rescue of specific astrocyte proteins that are reduced during epilepsy development and represent hallmarks of cell dysfunction (Devinsky et al., 2013). We measured by western blot $Kir_{4.1}$ and GLT-1 in the mouse hippocampus during reparixin treatment vs vehicle, as well as GFAP level as a marker of astrogliosis (Suppl. Fig. 4; $n = 5–7$). GLT-1 and $Kir_{4.1}$ proteins were down-regulated by 50% on average while GFAP levels were enhanced by 2-fold, thus confirming a reduced capacity of activated astrocytes to buffer extracellular K^+ and glutamate, modifications that are implicated in seizures (Coulter and Steinhäuser, 2015; Devinsky et al., 2013; Hubbard et al., 2016; Liu et al., 2020). Reparixin however did not prevent either the increase in GFAP or the decrease in Kir4.1 or GLT-1 levels in the hippocampus of mice, showing it did not rescue astroglial proteins expression.

3.5. Effect of reparixin on established spontaneous seizures

We next assessed whether reparixin affected established chronic seizures in epileptic mice using a new cohort of 18 mice exposed to SE, and randomized to drug treatment or vehicle ($n = 9$/group) after measuring their baseline of spontaneous seizures (1.5–2.0 months post-SE). Then, the same mice received either reparixin or vehicle for 2 consecutive weeks (2.0–2.5 months post-SE) followed by a 2-week washout period (2.5–3.0 months post-SE) (Fig. 4A).

Fig. 4**B** shows that reparixin significantly reduced the number of spontaneous seizures by 50% compared to respective pre-injection baseline ($p < 0.01$). Upon drug discontinuation, seizure number returned to pre-injection baseline value. The average duration of seizures was not modified by reparixin (*pre-injection baseline,* 48.2 ± 8.2 s; reparixin, 51.2 ± 13.0 s; washout, 56.4 ± 10.0 s). No significant changes in seizure number (Fig. 4**C**) or their average duration (*not shown*) were detected in parallel vehicle-treated mice during time-matched recording epochs.

In reparixin-treated mice, drug's plasma level positively correlated with the percentage of seizure reduction vs baseline ($r = 0.71$; $p = 0.02$ by Spearman two-tailed test).

3.6. CXCL1/ IL-8 and CXCR1/2 receptor expression

3.6.1. Epileptic mice

Immunohistochemical analysis of CXCL1 and its receptors was done in chronic epileptic mice ($n = 4$) and sham control mice ($n = 4$) (Suppl. Fig. 5). In sham mice, CXCL1 staining was detected in scattered CA1 and CA3 pyramidal cells and hilar interneurons (**A-C**). In epileptic mice, CXCL1 expression was increased in CA1 pyramidal cells (**D** vs **A**) and hilar (**F** vs **C**) neurons, but not in CA3 neurons (**E** vs **B**). CXCR1 receptor expression was detected in CA1 and CA3 pyramidal cells in sham mice (**A, B**), and this signal was increased in epileptic mice (**C,D**). CXCR1 immunoreactivity was also detected in scattered glial cells to a similar extent in sham and epileptic mice (*insets in* **A, C**). CXCR2 expression was barely detectable in sham mice in all hippocampal subfields (**A-C**) while it was increased in CA1 (**D** vs **A**), CA3 (**E** vs **B**) and hilar (**F** vs **C**) neurons in epileptic mice.

3.6.2. IL-8 and CXCR1/2 receptor expression in human temporal lobe epilepsy

Representative immunohistochemical images of the hippocampal regions are shown from patients with TLE with hippocampal sclerosis (TLE-HS; a condition mimicked by our murine model; Figs. 5 and 6) and without HS (TLE-no HS; Suppl. Figs. 6 and 7). Only hippocampal regions where the expression of the molecules of interest was significantly changed vs control tissue are depicted, while signal quantification is shown in box-and-whisker plots for each examined region.

IL-8. In control tissue, the chemokine displayed low cytoplasmic expression in neurons and was absent in glia in all hippocampal subfields (Fig. 5**A-D**). In TLE-HS patients (Fig. 5E-H), IL-8 expression was higher in neurons vs control tissue (*bargrams in panel* **I**) in CA1 (**E** vs **A**), GC (**F** vs **B**) and subiculum (**H** vs **D**) but not in the hilus (**G** vs **C**), while it did not differ in TLE-no HS vs control (Suppl. Fig. 6I). Moreover, astrocytes and microglia (*insets in* Fig. 5E) displayed stronger expression vs control in both TLE-HS (*arrowheads*; Fig. 5**E-H**vs **A-D**) and TLE-no HS (*arrowheads*; Suppl. Fig. 6**E-H** vs **A-D**) in all hippocampal subfields (*bargrams in* Fig. 5**J** and Suppl. Fig. 6**J**).

CXCR1. Neuronal cytoplasmatic expression was detected in control specimens (Fig. 6**A,C**) and did not significantly change in TLE-HS (Fig. 6**B,D** and *bargrams in* Fig. 6**E**). The faint CXCR1 cytoplasmic staining detected in glial cells in control tissue (Fig. 6**A,C**) was increased in both astrocytes and microglia in CA1 sector (*arrowheads*; *insets in* Fig. 6**B**) and in the hilus of dentate gyrus (*arrowheads*; Fig. 6**D**) in TLE-HS (*bargrams in* Fig. 6**F**). No changes in either neurons or glia were detected in TLE-no HS (*bargrams in* Suppl. Fig. 7**A, B**).

CXCR2. Faint expression of CXCR2 was detected in neuronal cytoplasm in control tissue (Fig. 6**G-I**); increased neuronal staining was found in CA1 of TLE-HS patients (Fig. 6J vs **G**) but not in the other subfields (panels **K,L** vs **H,I**; *bargrams in* Fig. 6M). In TLE-no HS, CXCR2 neuronal staining was increased only in the granule cell layer (Suppl. Fig. 7**D** vs **C** and *bargram in* panel **G**). Cytoplasmatic CXCR2 glia expression was barely detectable in control tissue (Fig. 6**G-I**). This glial cell signal was increased in microglia and astrocytes in CA1 (*arrowheads; insets in* Fig. 6**J**) and in the dentate gyrus (Fig. 6**K,L** vs **H,I**) of TLE-HS (*bargrams in* **N**). CXCR2 expression was also increased in the dentate gyrus of TLE-no HS (*arrowheads*; Suppl. Fig. 7**D,F** vs **C,E**; *bargrams in* **H**).

4. Discussion

Various chemokines and their receptors are increased in both parenchymal brain cells and leukocytes in human and experimental epilepsy (Cerri et al., 2017; de Vries et al., 2016; van Vliet et al., 2018). In addition to their role as chemotactic molecules that govern the tissue extravasation of peripheral immune cells, chemokines are endowed with neuromodulatory actions which make them potential candidates for altering neuronal network excitability in epilepsy. For example, fractalkine (CX3CL1) was shown to reduce GABAA use-dependent receptor

desensitization (i.e., rundown), as shown in oocytes transfected with human TLE membranes (Roseti et al., 2013), suggesting it reduces excitability by stabilizing receptor currents. On the contrary, the CCL2/MIP-2-CCR2 axis is involved in seizure generation since inhibition of CCL2 or blockade of CXCR2 receptors reduced seizures that were exacerbated by a systemic inflammatory challenge in epileptic mice (Cerri et al., 2016). This chemokine was also shown to contribute to SE-induced neuronal death (Tian et al., 2017). Similarly, reduction of CCR5 expression in circulating leukocytes reduced acute excitotoxic seizures in rats (Louboutin et al., 2011; Tian et al., 2017).

These data, together with the reported changes in chemokines level in brain and biofluids in epilepsy patients, support a potential involvement of chemokine signaling networks in the pathophysiology of seizures.

In this context, we provide new evidence for the ictogenic properties of CXCL1-CXCR1/2 receptor axis in a murine model of acquired epilepsy mimicking TLE-HS. First, we showed that the chemokine is increased in brain tissue, but not in blood, of mice that experienced SE and consequently developed epilepsy. Notably, the correspondent human chemokine IL-8 was reported to increase more strikingly in CSF than in blood, of patients with new onset refractory SE (NORSE) and drug-resistant epilepsy (Kenney-Jung et al., 2016; Sakuma et al., 2014). This set of data therefore supports an intracerebral CXCL1/IL-8 production in epilepsy. In accordance, we provide immunohistochemical evidence for increased CXCL1 expression in hippocampal CA1 and hilar interneurons in epileptic mice with sclerotic hippocampi, and similarly, IL-8 expression was increased in neurons in human TLE-HS foci. Noteworthy, no change in neuronal IL-8 expression was detected in human TLE without HS, suggesting that the specific neuropathology plays a role in chemokine up-regulation in neurons. In accord, enhanced IL-8 expression was reported in cortical brain regions of pronounced cell death in patients with drug-resistant epilepsy (Choi et al., 2009). In contrast, IL-8 was similarly enhanced in glial cells in both sclerotic and non-sclerotic human TLE hippocampi (*see also* Pernhorst et al., 2013), suggesting that glial upregulation is independent of histopathology, and does not simply reflect astrogliosis which is specific to HS, but it may be driven by seizures. We did not detect glial chemokine expression in epileptic mice which may be due to species difference or to the sensitivity for signal detection of the different antibodies used in human vs mouse brain.

We identified the target cells of CXCL1/IL-8 by assessing CXCR1 and CXCR2 receptor expression in the same brain tissue where the chemokine was induced. Immunohistochemical analysis of human hippocampal specimens showed that both receptors were expressed by neurons and glia (Liu et al., 2020). Semi-quantitative analysis showed a more prominent up-regulation of CXCR2 over CXCR1 in TLE vs control tissue. CXCR1 was induced only in TLE-HS and specifically in glia, while CXCR2 was up-regulated in TLE with and without HS, both in neurons and glia. In epileptic mice, we confirmed neuronal expression of both receptors in pyramidal cells but only CXCR1 was expressed by glia. In accordance, neuronal expression of CXCR2 was previously reported in the temporal cortex of human TLE and in epileptic mice exposed to pilocarpine (Xu et al., 2017) while no data were as yet available on CXCR1 expression in brain.

The predominant neuronal expression of CXCR1 and CXCR2 receptors in epileptic mice suggests that the ictogenic effects of brain-borne CXCL1 are mediated by neuronal cells. However, we cannot exclude that functional receptors are expressed by glia (i.e. CXCR1) or by brain vessels (Liu et al., 2020) and are involved in CXCL1 effects, although we did not detect receptor expression in vessel in our model.

Both neuronal and glial effects of CXCL1 have been reported which may be relevant for its involvement in seizures. In particular, CXCL1 enhances synaptic transmission (Cui et al., 2012) and can induce intracellular Ca^{2+} elevation (Deftu et al., 2018; Qin et al., 2005) and increases Na^{+} currents in neurons (Wang et al., 2008), and these effects were associated with enhanced neuronal excitability. The CXCL1-CXCR2 axis contributes to inflammatory pain by activation of neuronal NMDAR in the spinal cord (Cao et al., 2014; Yang et al., 2016), and CXCR2 regulates the functional properties of GLUR1 receptor (Lax et al., 2002), which contributes to seizures (Hanada, 2020).

The CXCL1-CXCR2 axis was also shown to induce astrogliosis, and to decrease astrocytic GLT-1 mediated glutamate uptake, contributing to acute pentylenetetrazol seizures (Liu et al., 2020). Our data do not support that reparixin's anti-seizure effect is mediated by rescue of astrocytic dysfunction as it did not affect $Kir_{4.1}$ and GLT-1 protein decrease during early disease development. However, we cannot exclude that blockade of CXCL1 receptors has indeed improved the function of the residual GLT-1, $Kir_{4.1}$ proteins, thus limiting cell loss and seizures (Devinsky et al., 2013; Liu et al., 2020).

Overall, the described CXCL1-mediated effects may decrease the seizure threshold, thereby contributing to seizure generation. Accordingly, reparixin reduced both acute and chronic seizures by 50% in mice during the treatment period, a clinically relevant endpoint (Perucca, 2018). This effect elapsed upon drug discontinuation, suggesting that reparixin has acute anti-ictogenic effects, and that endogenous CXCL1 plays a role in the mechanisms of ictogenesis.

Reparixin was administered to mice before SE in order to reach steady-state drug plasma concentration and attain the predicted therapeutic concentrations for preventing the effects of CXCL1, which increases in brain within 24 h from SE onset. Although our findings argue against a prolonged disease-modifying effect of reparixin, we cannot exclude that a longer treatment, either after SE or in the chronic epilepsy phase, might have resulted in lasting effects persisting beyond drug discontinuation. This might occur if only prolonged blockade of CXCL1-mediated signaling would impact epileptogenesis and mediate disease-modifying effects. Further studies testing different timing of drug administration are needed to elucidate these aspects, and for more closely mimicking the clinical intervention. In this context, anti-epileptogenic effects of CXCL1 were reported using a specific CXCR2 antagonist administered for 2 weeks after SE in pilocarpine-injected mice (Xu et al., 2017) where spontaneous seizure reduction was observed 7 days after treatment discontinuation.

Only behavioral seizures were monitored in the Xu et al. (2017) study, therefore it is unclear if the CXCR2 receptor antagonist reduced the motor component of seizures by limiting seizure generalization, or also decreased EEG seizure activity like in our study. Since we did not monitor motor seizures in our mice, the comparison between the two treatments remains speculative.

Reparixin shows a limited BBB penetration in healthy animals but still compatible with the attainment of pharmacologically effective concentrations in the brain tissue (12–24 nM) in our experimental setting. In accord, reparixin was able to prevent the acetylation of α-tubulin induced by SE in the hippocampus, which is a pharmacodynamic index of reparixin's action (Brandolini et al., 2017). This evidence, together with the brain-specific increase of CXCL1 and the upregulation of CXCR1/2 receptors in neurons, supports that reparixin has intracerebral effects.

BBB damage observed in our epilepsy model and other injury models (Brandolini et al., 2015; Garau et al., 2005) might also facilitate brain penetration of the free compound. However, since the drug is mostly bound to serum albumin, the BBB leakage does not necessarily imply that reparixin enters the brain at higher effective concentrations (Löscher and Friedman, 2020).

Hippocampal leukocyte extravasation was reduced in mice treated with reparixin during the early disease phase. This phenomenon was associated with reduced CA1 hippocampal cell loss in similar epilepsy models (Varvel et al., 2021, 2016; Zattoni et al., 2011), suggesting it may play a role in neuroprotection in drug-treated mice.

In conclusion, the contribution of CXCL1 to acute and chronic seizures in mice, together with evidence of elevated IL-8 in the CSF of patients with drug-resistant epilepsy and NORSE, suggests that IL-8 represents a new therapeutic target to attain anticonvulsive effects in

humans. Notably, in the context of potential therapeutics that inhibit chemokine activity, reparixin is an investigational drug with a safe and well-tolerated profile as demonstrated in phase II and phase III clinical studies (Goldstein et al., 2020; Maffi et al., 2020; Opfermann et al., 2015). Additionally, reparixin is currently investigated in a multicenter phase 3 study in patients with severe COVID19 pneumonia, therefore prompting further studies on its potential therapeutic effects in epilepsy patients with drug-resistant seizures.

Supplementary data to this article can be found online at https://doi.org/10.1016/j.nbd.2021.105468.

Author contributions

Rossella Di Sapia carried out the in vivo pharmacological experiments and contributed to design the experimental plan; Valentina Kebede contributed to the in vivo experiments; Till S. Zimmer carried out the studies in human tissue, and together with Eleonora Aronica described and discussed the related results; Teresa Ravizza carried out the immunohistochemical analyses in the animal model; Diletta Sorrentino and Manuel Alejandro Montano Castillo contributed to the immunohistochemistry; Silvia Balosso carried out the western blot studies; Luca Porcu performed the statistical analysis of data; Franca Cattani carried out the reparixin and CXCL1 measurements; Marcello Allegretti, Laura Brandolini and Annamaria Vezzani developed the experimental plan and designed the treatment schedule; Annamaria Vezzani wrote the manuscript with the main contribution of Rossella Di Sapia, Teresa Ravizza, Laura Brandolini, and the partecipation of Till S Zimmer, Silvia Balosso, Eleonora Aronica and Marcello Allegretti.

Declaration of Competing Interest

Laura Brandolini, Franca Cattani, Anna Ruocco and Marcello Allegretti are employed by Dompe' Farmaceutici S.p.a. The other authors declare no conflict of interest.

Acknowledgements

The authors thank the contribution of Dr. V. Iori and Dr C. Kostoula in the initial phases of this study. This preclinical study was supported by an unrestricted grant to A.V. from Dompe' Farmaceutici S.p.a. Human tissue study was supported by a grant to E.A. from the European Union's Horizon 2020 research and innovation program under the Marie Sklodowska-Curie grant agreement no. 722053 (EU-GliaPhD; TSZ, EA) and no. 952455 (EpiEpiNet; AE),

References

Arena, A., Zimmer, T.S., van Scheppingen, J., Korotkov, A., Anink, J.J., Mühlebner, A., Jansen, F.E., van Hecke, W., Spliet, W.G., van Rijen, P.C., Vezzani, A., Baayen, J.C., Idema, S., Iyer, A.M., Perluigi, M., Mills, J.D., van Vliet, E.A., Aronica, E., 2019. Oxidative stress and inflammation in a spectrum of epileptogenic cortical malformations: molecular insights into their interdependence. Brain Pathol. 29, 351–365.

Baggiolini, M., 1998. Chemokines and leukocyte traffic. Nature 392, 565–568.

Bartolini, L., Piras, E., Sullivan, K., Gillen, S., Bumbut, A., Lin, C.-T.M., Leibovitch, E.C., Graves, J.S., Waubant, E.L., Chamberlain, J.M., Gaillard, W.D., Jacobson, S., 2018. Detection of HHV-6 and EBV and cytokine levels in saliva from children with seizures: results of a multi-center Cross-sectional study. Front. Neurol. 9, 834.

Bertini, R., Allegretti, M., Bizzarri, C., Moriconi, A., Locati, M., Zampella, G., Cervellera, M.N., Di Cioccio, V., Cesta, M.C., Galliera, E., Martinez, F.O., Di Bitondo, R., Troiani, G., Sabbatini, V., D'Anniballe, G., Anacardio, R., Cutrin, J.C., Cavalieri, B., Mainiero, F., Strippoli, R., Villa, P., Di Girolamo, M., Martin, F., Gentile, M., Santoni, A., Corda, D., Poli, G., Mantovani, A., Ghezzi, P., Colotta, F., 2004. Noncompetitive allosteric inhibitors of the inflammatory chemokine receptors CXCR1 and CXCR2: prevention of reperfusion injury. Proc. Natl. Acad. Sci. U. S. A. 101, 11791–11796.

Blumcke, I., Thom, M., Aronica, E., Armstrong, D.D., Bartolomei, F., Bernasconi, A., Bernasconi, N., Bien, C.G., Cendes, F., Coras, R., Cross, J.H., Jacques, T.S., Kahane, P., Mathern, G.W., Miyata, H., Moshe, S.L., Oz, B., Ozkara, C., Perucca, E., Sisodiya, S., Wiebe, S., Spreafico, R., 2013. International consensus classification of hippocampal sclerosis in temporal lobe epilepsy: a task force report from the ILAE commission on diagnostic methods. Epilepsia 54, 1315–1329.

Brandolini, L., Cristiano, L., Fidoamore, A., De Pizzol, M., Di Giacomo, E., Florio, T.M., Confalone, G., Galante, A., Cinque, B., Benedetti, E., Ruffini, P.A., Cifone, M.G., Giordano, A., Alecci, M., Allegretti, M., Cimini, A., 2015. Targeting CXCR1 on breast cancer stem cells: signaling pathways and clinical application modelling. Oncotarget 6, 43375–43394.

Brandolini, L., Benedetti, E., Ruffini, P.A., Russo, R., Cristiano, L., Antonosante, A., d'Angelo, M., Castelli, V., Giordano, A., Allegretti, M., Cimini, A., 2017. CXCR1/2 pathways in paclitaxel-induced neuropathic pain. Oncotarget 8, 23188–23201.

Cao, D.-L., Zhang, Z.-J., Xie, R.-G., Jiang, B.-C., Ji, R.-R., Gao, Y.-J., 2014. Chemokine CXCL1 enhances inflammatory pain and increases NMDA receptor activity and COX-2 expression in spinal cord neurons via activation of CXCR2. Exp. Neurol. 261, 328–336.

Cavalieri, B., Mosca, M., Ramadori, P., Perrelli, M.-G., De Simone, L., Colotta, F., Bertini, R., Poli, G., Cutrìn, J.C., 2005. Neutrophil recruitment in the reperfused-injured rat liver was effectively attenuated by repertaxin, a novel allosteric noncompetitive inhibitor of CXCL8 receptors: a therapeutic approach for the treatment of post-ischemic hepatic syndromes. Int. J. Immunopathol. Pharmacol. 18, 475–486.

Cerri, C., Genovesi, S., Allegra, M., Pistillo, F., Puntener, U., Guglielmotti, A., Perry, V.H., Bozzi, Y., VCaleo, M., 2016. The chemokine CCL2 mediates the seizure-enhancing effects of systemic inflammation. J. Neurosci. 36, 3777–3788.

Cerri, C., Caleo, M., Bozzi, Y., 2017. Chemokines as new inflammatory players in the pathogenesis of epilepsy. Epilepsy Res. 136, 77–83.

Choi, J., Nordli, D.R., Alden, T.D., DiPatri, A., Laux, L., Kelley, K., Rosenow, J., Schuele, S.U., Rajaram, V., Koh, S., 2009. Cellular injury and neuroinflammation in children with chronic intractable epilepsy. J. Neuroinflammation 6, 38.

Coulter, D.A., Steinhäuser, C., 2015. Role of astrocytes in epilepsy. Cold Spring Harb Perspect Med 5, a022434.

Cui, G., An, J., Zhang, N., Zhao, M., Liu, S., Yi, J., 2012. Elevated interleukin-8 enhances prefrontal synaptic transmission in mice with persistent inflammatory pain. Mol. Pain 8, 11.

De Herdt, V., Bogaert, S., Bracke, K.R., Raedt, R., De Vos, M., Vonck, K., Boon, P., 2009. Effects of vagus nerve stimulation on pro- and anti-inflammatory cytokine induction in patients with refractory epilepsy. J. Neuroimmunol. 214, 104–108.

de Vries, E.E., van den Munckhof, B., Braun, K.P.J., van Royen-Kerkhof, A., de Jager, W., Jansen, F.E., 2016. Inflammatory mediators in human epilepsy: a systematic review and meta-analysis. Neurosci. Biobehav. Rev. 63, 177–190.

Deftu, A.F., Filippi, A., Gheorghe, R.O., Ristoiu, V., 2018. CXCL1 activates TRPV1 via Gi/o protein and actin filaments. Life Sci. 193, 282–291.

Devinsky, O., Vezzani, A., Najjar, S., De Lanerolle, N.C., Rogawski, M.A., 2013. Glia and epilepsy: excitability and inflammation. Trends Neurosci. 36, 174–184.

Di Nunzio, M., Di Sapia, R., Sorrentino, D., Kebede, V., Cerovic, M., Gullotta, G.S., Bacigaluppi, M., Audinat, E., Marchi, N., Ravizza, T., Vezzani, A., 2021. Microglia proliferation plays distinct roles in acquired epilepsy depending on disease stages. Epilepsia. https://doi.org/10.1111/epi.16956. Online ahead of print.

Franklin, K.B.J., Paxinos, G., 2008. The Mouse Brain in Stereotaxic Coordinates. Academic Press, San Diego.

Frigerio, F., Flynn, C., Han, Y., Lyman, K., Lugo, J.N., Ravizza, T., Ghestem, A., Pitsch, J., Becker, A., Anderson, A.E., Vezzani, A., Chetkovich, D., Bernard, C., 2018a. Neuroinflammation alters integrative properties of rat hippocampal pyramidal cells. Mol. Neurobiol. 55, 7500–7511.

Frigerio, F., Pasqualini, G., Craparotta, I., Marchini, S., van Vliet, E.A., Foerch, P., Vandenplas, C., Leclercq, K., Aronica, E., Porcu, L., Pistorius, K., Colas, R.A., Hansen, T.V., Perretti, M., Kaminski, R.M., Dalli, J., Vezzani, A., 2018b. N-3 Docosapentaenoic acid-derived protectin D1 promotes resolution of neuroinflammation and arrests epileptogenesis. Brain 141, 3130–3143.

Gallentine, W.B., Shinnar, S., Hesdorffer, D.C., Epstein, L., Nordli, D.R., Lewis, D.V., Frank, L.M., Seinfeld, S., Shinnar, R.C., Cornett, K., Liu, B., Moshé, S.L., Sun, S., FEBSTAT Investigator Team, 2017. Plasma cytokines associated with febrile status epilepticus in children: a potential biomarker for acute hippocampal injury. Epilepsia 58, 1102–1111.

Garau, A., Bertini, R., Colotta, F., Casilli, F., Bigini, P., Cagnotto, A., Mennini, T., Ghezzi, P., Villa, P. 2005. Neuroprotection with the CXCL8 inhibitor repertaxin in transient brain ischemia. Cytokine 30, 125–31.

Goldstein, L.J., Perez, R.P., Yardley, D., Han, L.K., Reuben, J.M., Gao, H., McCanna, S., Butler, B., Ruffini, P.A., Liu, Y., Rosato, R.R., Chang, J.C., 2020. A window-of-opportunity trial of the CXCR1/2 inhibitor reparixin in operable HER-2-negative breast cancer. Breast Cancer Res. 22, 4.

Hanada, T., 2020. Ionotropic glutamate receptors in epilepsy: a review focusing on AMPA and NMDA receptors. Biomolecules 10, 464.

Hubbard, J.A., Szu, J.I., Yonan, J.M., Binder, D.K., 2016. Regulation of astrocyte glutamate transporter-1 (GLT1) and aquaporin-4 (AQP4) expression in a model of epilepsy. Exp. Neurol. 283, 85–96.

Hutchinson, E., Avery, A., Vandewoude, S., 2005. Environmental enrichment for laboratory rodents. ILAR J. 46, 148–161.

Iori, V., Iyer, A.M., Ravizza, T., Beltrame, L., Paracchini, L., Marchini, S., Cerovic, M., Hill, C., Ferrari, M., Zucchetti, M., Molteni, M., Rossetti, C., Brambilla, R., Steve White, H., D'Incalci, M., Aronica, E., Vezzani, A., 2017. Blockade of the IL-1R1/TLR4 pathway mediates disease-modification therapeutic effects in a model of acquired epilepsy. Neurobiol. Dis. 99, 12–23.

Ito, R., Katano, I., Kawai, K., Yagoto, M., Takahashi, T., Ka, Y., Ogura, T., Takahashi, R., Ito, M., 2017. A novel xenogeneic graft-versus-host disease model for investigating the pathological role of human CD4(+) or CD8(+) T cells using Immunodeficient NOG mice. Am. J. Transplant. 17, 1216–1228.

Kenney-Jung, D.L., Vezzani, A., Kahoud, R.J., LaFrance-Corey, R.G., Ho, M.L., Muscardin, T.W., Wirrell, E.C., Howe, C.L., Payne, E.T., 2016. Febrile infection-related epilepsy syndrome treated with anakinra. Ann. Neurol. 80, 939–945.
Kilkenny, C., Browne, W.B., Cuthill, I.C., Emerson, M., Altman, D.G., 2010. Perspective improving bioscience research reporting: The ARRIVE guidelines for reporting animal research. PLoS Biol. 8 e1000412.
Lax, P., Limatola, C., Fucile, S., Trettel, F., Di Bartolomeo, S., Renzi, M., Ragozzino, D., Eusebei, F., 2002. Chemokine receptor CXCR2 regulates the functional properties of AMPA-type glutamate receptor GluR1 in HEK cells. J. Neuroimmunol. 129, 66–73.
Liu, X.-X., Yang, L., Shao, L.-X., He, Y., Wu, G., Bao, Y.-H., Lu, N.-N., Gong, D.-M., Lu, Y.-P., Cui, T.-T., Sun, N.-H., Chen, D.-Y., Shi, W.-X., Fukunaga, K., Chen, H.-S., Chen, Z., Han, F., Lu, Y.-M., 2020. Endothelial Cdk5 deficit leads to the development of spontaneous epilepsy through CXCL1/CXCR2-mediated reactive astrogliosis. J. Exp. Med. 217.
Louboutin, J.-P., Chekmasova, A., Marusich, E., Agrawal, L., Strayer, D.S., 2011. Role of CCR5 and its ligands in the control of vascular inflammation and leukocyte recruitment required for acute excitotoxic seizure induction and neural damage. FASEB J. 25, 737–753.
Löscher, W., Friedman, A., 2020. Structural, Molecular, and Functional Alterations of the Blood-Brain Barrier during Epileptogenesis and Epilepsy: A Cause, Consequence, or Both? Int. J. Mol. Sci. 21, 591.
Maffi, P., Lundgren, T., Tufveson, G., Rafael, E., Shaw, J.A.M., Liew, A., Saudek, F., Witkowski, P., Golab, K., Bertuzzi, F., Gustafsson, B., Daffonchio, L., Ruffini, P.A., Piemonti, L., REP0211 Study Group, 2020. Targeting CXCR1/2 does not improve insulin secretion after pancreatic islet transplantation: a phase 3, double-blind, randomized, placebo-controlled trial in type 1 diabetes. Diabetes Care 43, 710–718.
Morin-Brureau, M., Milior, G., Royer, J., Chali, F., Le Duigou, C., Savary, E., Blugeon, C., Jourdren, L., Akbar, D., Dupont, S., Navarro, V., Baulac, M., Bielle, F., Mathon, B., Clemenceau, S., Miles, R., 2018. Microglial phenotypes in the human epileptic temporal lobe. Brain 141, 3343–3360.
Mouri, G., Jimenez-Mateos, E., Engel, T., Dunleavy, M., Hatazaki, S., Paucard, A., Matsushima, S., Taki, W., Henshall, D.C., 2008. Unilateral hippocampal CA3-predominant damage and short latency epileptogenesis after intra-amygdala microinjection of kainic acid in mice. Brain Res. 1213, 140–151.
Opfermann, P., Derhaschnig, U., Felli, A., Wenisch, J., Santer, D., Zuckermann, A., Dworschak, M., Jilma, B., Steinlechner, B., 2015. A pilot study on reparixin, a CXCR1/2 antagonist, to assess safety and efficacy in attenuating ischaemia-reperfusion injury and inflammation after on-pump coronary artery bypass graft surgery. Clin. Exp. Immunol. 180, 131–142.
Pascente, R., Frigerio, F., Rizzi, M., Porcu, L., Boido, M., Davids, J., Zaben, M., Tolomeo, D., Filibian, M., Gray, W.P., Vezzani, A., Ravizza, T., 2016. Cognitive deficits and brain myo-inositol are early biomarkers of epileptogenesis in a rat model of epilepsy. Neurobiol. Dis. 93, 146–155.
Pasetto, L., Pozzi, S., Castelnovo, M., Basso, M., Estevez, A.G., Fumagalli, S., De Simoni, M.G., Castellaneta, V., Bigini, P., Restelli, E., Chiesa, R., Trojsi, F., Monsurrò, M.R., Callea, L., Malešević, M., Fischer, G., Freschi, M., Tortarolo, M., Bendotti, C., Bonetto, V., 2017. Targeting extracellular Cyclophilin a reduces Neuroinflammation and extends survival in a mouse model of amyotrophic lateral sclerosis. J. Neurosci. 37, 1413–1427.
Pernhorst, K., Herms, S., Hoffmann, P., Cichon, S., Schulz, H., Sander, T., Schoch, S., Becker, A.J., Grote, A., 2013. TLR4, ATF-3 and IL8 inflammation mediator expression correlates with seizure frequency in human epileptic brain tissue. Seizure 22, 675–678.
Perucca, E., 2018. From clinical trials of antiepileptic drugs to treatment. Epilepsia Open 3, 220–230.
Pollard, J.R., Eidelman, O., Mueller, G.P., Dalgard, C.L., Crino, P.B., Anderson, C.T., Brand, E.J., Burakgazi, E., Ivaturi, S.K., Pollard, H.B., 2013. The TARC/sICAM5 ratio in patient plasma is a candidate biomarker for drug resistant epilepsy. Front. Neurol. 3, 181.
Qin, X., Wan, Y., Wang, X., 2005. CCL2 and CXCL1 trigger calcitonin gene-related peptide release by exciting primary nociceptive neurons. J. Neurosci. Res. 82, 51–62.
Raja, U.M., Gopal, G., Shirley, S., Ramakrishnan, A.S., Rajkumar, T., 2017. Immunohistochemical expression and localization of cytokines/chemokines/growth factors in gastric cancer. Cytokine 89, 82–90.
Rawat, C., Kushwaha, S., Srivastava, A.K., Kukreti, R., 2020. Peripheral blood gene expression signatures associated with epilepsy and its etiologic classification. Genomics 112, 218–224.
Roseti, C., Fucile, S., Lauro, C., Martinello, K., Bertollini, C., Esposito, V., Mascia, A., Catalano, M., Aronica, E., Limatola, C., Palma, E., 2013. Fractalkine/CX3CL1 modulates GABAA currents in human temporal lobe epilepsy. Epilepsia 54, 1834–1844.
Rüber, T., David, B., Lüchters, G., Nass, R.D., Friedman, A., Surges, R., Stöcker, T., Weber, B., Deichmann, R., Schlaug, G., Hattingen, E., Elger, C.E., 2018. Evidence for peri-ictal blood-brain barrier dysfunction in patients with epilepsy. Brain 141, 2952–2965.
Sakuma, H., Tanuma, N., Kuki, I., Takahashi, Y., Shiomi, M., Hayashi, M., 2014. Intrathecal overproduction of proinflammatory cytokines and chemokines in febrile infection-related refractory status epilepticus. J. Neurol. Neurosurg. Psychiatry 86, 820–822.
Souza, D.G., Bertini, R., Vieira, A.T., Cunha, F.Q., Poole, S., Allegretti, M., Colotta, F., Teixeira, M.M., 2004. Repertaxin, a novel inhibitor of rat CXCR2 function, inhibits inflammatory responses that follow intestinal ischaemia and reperfusion injury. Br. J. Pharmacol. 143, 132–142.
Strauss, K.I., Elisevich, K.V., 2016. Brain region and epilepsy-associated differences in inflammatory mediator levels in medically refractory mesial temporal lobe epilepsy. J. Neuroinflammation 13, 270.
Taalab, M., Mohammed, W.F., Helmy, M.A., Othman, A.A.A., Darwish, M., Hassan, I., Abbas, M., 2019. Cannabis influences the putative cytokines-related pathway of epilepsy among Egyptian epileptic patients. Brain Sci 9, 332.
Terrone, G., Pauletti, A., Salamone, A., Rizzi, M., Villa, B.R., Porcu, L., Sheehan, M.J., Guilmette, E., Butler, C.R., Piro, J.R., Samad, T.A., Vezzani, A., 2018. Inhibition of monoacylglycerol lipase terminates diazepam-resistant status epilepticus in mice and its effects are potentiated by a ketogenic diet. Epilepsia 59, 79–91.
Tian, D.-S., Peng, J., Murugan, M., Feng, L.-J., Liu, J.-L., Eyo, U.B., Zhou, L.-J., Mogilevsky, R., Wang, W., Wu, L.-J., 2017. Chemokine CCL2-CCR2 signaling induces neuronal cell death via STAT3 activation and IL-1β production after status Epilepticus. J. Neurosci. 37, 7878–7892.
van Vliet, E.A., Aronica, E., Vezzani, A., Ravizza, T., 2018. Review: Neuroinflammatory pathways as treatment targets and biomarker candidates in epilepsy: emerging evidence from preclinical and clinical studies. Neuropathol. Appl. Neurobiol. 44, 91–111.
Varvel, N.H., Neher, J.J., Bosch, A., Wang, W., Ransohoff, R.M., Miller, R.J., Dingledine, R., 2016. Infiltrating monocytes promote brain inflammation and exacerbate neuronal damage after status epilepticus. Proc. Natl. Acad. Sci. U. S. A. 113, E5665–E5674.
Varvel, N.H., Espinosa-Garcia, C., Hunter-Chang, S., Chen, D., Biegel, A., Hsieh, A., Blackmer-Raynolds, L., Ganesh, T., Dingledine, R., 2021. Peripheral myeloid cell EP2 activation contributes to the deleterious consequences of status Epilepticus. J. Neurosci. 41, 1105–1117.
Vezzani, A., Viviani, B., 2015. Neuromodulatory properties of inflammatory cytokines and their impact on neuronal excitability. Neuropharmacology 96, 70–82.
Vezzani, A., Balosso, S., Ravizza, T., 2019. Neuroinflammatory pathways as treatment targets and biomarkers in epilepsy. Nat. Rev. Neurol. 15, 459–472.
Wang, J.-G., Strong, J.A., Xie, W., Yang, R.-H., Coyle, D.E., Wick, D.M., Dorsey, E.D., Zhang, J.-M., 2008. The chemokine CXCL1/growth related oncogene increases sodium currents and neuronal excitability in small diameter sensory neurons. Mol. Pain 4, 38.
Xu, T., Yu, X., Wang, T., Liu, Y., Liu, X., Ou, S., Chen, Y., 2017. The effect of CXCR2 inhibition on seizure activity in the pilocarpine epilepsy mouse model. Brain Res. Bull. 134, 91–98.
Yang, L.-H., Xu, G.-M., Wang, Y., 2016. Up-regulation of CXCL1 and CXCR2 contributes to remifentanil-induced hypernociception via modulating spinal NMDA receptor expression and phosphorylation in rats. Neurosci. Lett. 626, 135–141.
Zarbock, A., Allegretti, M., Ley, K., 2008. Therapeutic inhibition of CXCR2 by Reparixin attenuates acute lung injury in mice. Br. J. Pharmacol. 155, 357–364.
Zattoni, M., Mura, M.L., Deprez, F., Schwendener, R.A., Engelhardt, B., Frei, K., Fritschy, J.M., 2011. Brain infiltration of leukocytes contributes to the pathophysiology of temporal lobe epilepsy. J. Neurosci. 31, 4037–4050.